Article

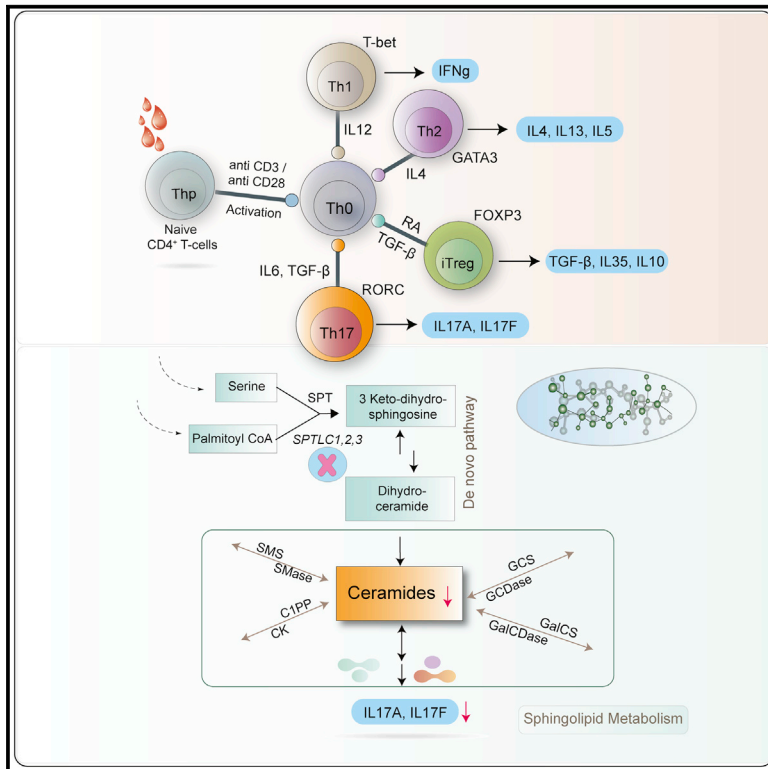# Quantitative genome-scale metabolic modeling of human CD4+ T cell differentiation reveals subset-specific regulation of glycosphingolipid pathways

Graphical abstract

Authors

Partho Sen, Syed Bilal Ahmad Andrabi, Tanja Buchacher, ..., Tuulia Hyötyläinen, Riitta Lahesmaa, Matej Orešič

Correspondence

partho.sen@utu.fi (P.S.),
riitta.lahesmaa@utu.fi (R.L.),
matej.oresic@oru.se (M.O.)

In brief

Sen et al. combine genome-scale metabolic modeling and multiomics datasets to identify the metabolic pathways involved in the activation and functional differentiation of human CD4+ T cell subsets (Th1, Th2, Th17, and iTreg cells). The study reveals the importance of ceramide and glycosphingolipid pathways in Th17 differentiation and effector functions.

Highlights

- T cells undergo metabolic reprogramming upon activation and differentiation

- Metabolic signatures of human CD4+ T cell subsets are identified

- Dysregulation of ceramides and glycosphingolipid pathways can alter Th17 functions

- The *de novo* sphingolipid pathway modulates expression of IL-17A and IL-17F in Th17 cells

CellPress

Cell Reports

Article

Quantitative genome-scale metabolic modeling of human CD4+ T cell differentiation reveals subset-specific regulation of glycosphingolipid pathways

Partho Sen,[1,2,*] Syed Bilal Ahmad Andrabi,[1] Tanja Buchacher,[1] Mohd Moin Khan,[1] Ubaid Ullah Kalim,[1]
Tuomas Mikael Lindeman,[1] Marina Amaral Alves,[1] Victoria Hinkkanen,[1] Esko Kemppainen,[1] Alex M. Dickens,[1,3]
Omid Rasool,[1] Tuulia Hyötyläinen,[4] Riitta Lahesmaa,[1,*] and Matej Orešič[1,2,5,*]
[1]Turku Bioscience Centre, University of Turku and Åbo Akademi University, 20520 Turku, Finland
[2]School of Medical Sciences, Örebro University, 702 81 Örebro, Sweden
[3]Department of Chemistry, University of Turku, 20520 Turku, Finland
[4]School of Science and Technology, Örebro University, Örebro, Sweden
[5]Lead contact
*Correspondence: partho.sen@utu.fi (P.S.), riitta.lahesmaa@utu.fi (R.L.), matej.oresic@oru.se (M.O.)
https://doi.org/10.1016/j.celrep.2021.109973

SUMMARY

T cell activation, proliferation, and differentiation involve metabolic reprogramming resulting from the interplay of genes, proteins, and metabolites. Here, we aim to understand the metabolic pathways involved in the activation and functional differentiation of human CD4+ T cell subsets (T helper [Th]1, Th2, Th17, and induced regulatory T [iTreg] cells). Here, we combine genome-scale metabolic modeling, gene expression data, and targeted and non-targeted lipidomics experiments, together with *in vitro* gene knockdown experiments, and show that human CD4+ T cells undergo specific metabolic changes during activation and functional differentiation. In addition, we confirm the importance of ceramide and glycosphingolipid biosynthesis pathways in Th17 differentiation and effector functions. Through *in vitro* gene knockdown experiments, we substantiate the requirement of serine palmitoyltransferase (*SPT*), a *de novo* sphingolipid pathway in the expression of proinflammatory cytokines (interleukin [IL]-17A and IL17F) by Th17 cells. Our findings provide a comprehensive resource for selective manipulation of CD4+ T cells under disease conditions characterized by an imbalance of Th17/natural Treg (nTreg) cells.

INTRODUCTION

CD4+ T cells orchestrate immune responses and mediate protective immunity against pathogens (Zhu and Paul, 2008). An aberrant T cell response is associated with cancer and autoimmune disorders (Kallionpää et al., 2019; Liblau et al., 2002; Nurieva et al., 2013). Circulating naive T helper cells are metabolically quiescent and predominantly use oxidative phosphorylation (OXPHOS) to fuel their biological processes (Chang and Pearce, 2016; Dimeloe et al., 2017; Macintyre and Rathmell, 2013; MacIver et al., 2013). When exposed to antigens, naive T cells undergo activation, clonal expansion, and differentiation to various effector T (Teff) cells, including T helper (Th)1, Th2, Th17, and regulatory T (Treg) cells, each driving various aspects of the immune responses (O'Shea and Paul, 2010; Tuomela and Lahesmaa, 2013).

Upon activation, T cells undergo metabolic reprogramming in order to provide energy and biosynthetic intermediates for growth and effector functions (Buck et al., 2015; Chang and Pearce, 2016; MacIver et al., 2013; Pearce and Pearce, 2013; Sugiura and Rathmell, 2018). At this stage, aerobic glycolysis is augmented (the Warburg effect), which increases the activities

of glycolytic enzymes. Their extracellular uptake of glucose increases by 40%–50% (Coloff et al., 2011), which, in turn, enhances their lactate production. Concomitantly, oxygen (O_2) intake is increased by ∼60% (Calder, 1995), while the utilization of glucose via OXPHOS is reduced (Macintyre and Rathmell, 2013). Activated T cells induces a metabolic sensor, i.e., mammalian target of rapamycin (mTOR), to either differentiate into Teff cells or become suppressive Treg cells (Barbi et al., 2013). mTOR signaling induces the transcription factors Myc and HIF-1α, driving the expression of genes important for glycolysis and glutaminolysis as well as regulating STAT signaling for T cell differentiation (Powell and Delgoffe, 2010).

Dysregulation of metabolic reprogramming of T cells can impair their clonal expansion (Dimeloe et al., 2017; MacIver et al., 2013). Depletion of glutamine in *in vitro* culture markedly impairs proliferation and cytokine production of T cells (Carr et al., 2010). Increased intracellular L-arginine is also linked to metabolic regulation, survival, and the anti-tumor activity of T cells (Geiger et al., 2016). T cell subsets such as Th1, Th2, and Th17, require acetyl-coenzyme A (CoA) carboxylase I (*ACC1*) for maturation (Chang and Pearce, 2016). In mice, T cell-specific *ACC1* deletion, or inhibition by the inhibitor

soraphen A, prevents Th17 differentiation and cell-mediated autoimmune disease development (Berod et al., 2014).

Taken together, there is evidence that T cell activation, differentiation, and effector functions are intrinsically linked to metabolic pathways (Buck et al., 2015; Chang and Pearce, 2016; Chang et al., 2013; Gerriets and Rathmell, 2012; MacIver et al., 2013; Pearce and Pearce, 2013; Pearce et al., 2013; Puleston et al., 2021; Sugiura and Rathmell, 2018; Wagner et al., 2021). However, not much is known about the common and specific metabolic signatures in human CD4$^+$ T cells and their functional subsets. Such knowledge could enable the selective manipulation of metabolism in these cells, with relevance to specific disease conditions (O'Sullivan and Pearce, 2015).

Genome-scale metabolic models (GEMs) are computational frameworks that link genes, proteins/enzymes, metabolites, and pathways found in cells, tissues, organs, and organisms (Agren et al., 2012; Orth et al., 2010; Sen et al., 2018; Thiele and Palsson, 2010). During the past decade, genome-scale metabolic modeling (GSMM) has emerged as a powerful tool to study metabolism in human cells (Mardinoglu et al., 2014; Sen et al., 2018, 2020). GSMM allows us to infer mechanistic relationships between genotype and phenotype (Agren et al., 2012; Orth et al., 2010; Sen et al., 2018; Thiele and Palsson, 2010).

Here, we combined gene expression data, targeted and non-targeted lipidomics experiments, and *in vitro* gene silencing in order to build GEMs of human CD4$^+$ T cells and applied GSMM to understand how these immune cells modulate their metabolism during activation and subsequent functional differentiation. Our integrative approach identified several metabolic processes of interest. We reveal the essentiality of glycosphingolipid (GSL) pathways in Th17 cells and show that the sphingolipid metabolic pathways were altered in the CD4$^+$ T cells (Kallionpää et al., 2019) and peripheral blood mononuclear cells (PBMCs) (Kallionpää et al., 2019; Sen et al., 2020) of the children who developed islet autoantibodies.

RESULTS

HTimmR: A genome-scale metabolic reconstruction of human CD4$^+$ T cells

We developed "human T-immuno reconstructor" (HTimmR), a generic and consensus metabolic reconstruction of human CD4$^+$ T cells. HTimmR includes 3,841 metabolic genes (MGs), 7,558 reactions, and 5,140 metabolites. HTimmR includes eight cellular compartments, i.e., extracellular cavity, peroxisome, mitochondria, cytosol, lysosome, endoplasmic reticulum, Golgi apparatus, and nucleus, as well as a cellular boundary that mimics a CD4$^+$ T cell. HTimmR was contextualized, i.e., the active metabolic reactions in the model were selected using the gene expression data (see STAR Methods). Cell-type functional GEMs for T naive (T helper precursor [Thp]), Th1, Th2, Th17, and induced Treg (iTreg) cells were developed (Figure 1A).

Identification of MGs of human CD4$^+$ T cell activation and subset differentiation

When mapping the published gene expression data of each CD4$^+$ T cell subset (i.e., Thp, Th1, and Th2 [Kanduri et al., 2015], Th17 [Tuomela et al., 2016], and iTreg cells [Ubaid Ullah

et al., 2018]) to the various available human metabolic reconstructions and pathway databases (see STAR Methods), we found that approximately 17% of the genes expressed in each CD4$^+$ T cell subset were found in the human metabolic reaction (HMR2) (Mardinoglu et al., 2014) database, while only ~5% of the genes were found in the Kyoto Encyclopedia of Genes and Genomes (KEGG) (Kanehisa and Goto, 2000) and the Encyclopedia of Human Genes and Metabolism (HumanCyc) (Trupp et al., 2010) pathway databases (Figure S1). The mapped genes for each CD4$^+$ T cell subset were assembled and listed as MGs. A total of 638 MGs were common to both the human metabolic reconstructions and metabolic pathway databases, while 750 MGs were unique to HMR2 (Figure 1B). Since HMR2 had the highest coverage of MGs in our CD4$^+$ T cell datasets, it was used as a background model for the reconstruction of HTimmR.

When we investigated the differential expression of MGs between naive (Thp), activated (Th0), and differentiated CD4$^+$ T cell subsets, we found that 853 MGs were differentially expressed (adjusted p [p.adj] < 0.05, adjusted for false discovery rate [FDR]), i.e., upregulated or downregulated in Th0 cells as compared to Thp cells (Figure S1). Similarly, 173, 506, 106, and 99 MGs were differentially expressed (p.adj < 0.05) between Th1, Th2, Th17, and iTreg cells, respectively, as compared to Th0 cells at 72 h of polarization (Figure S1). Gene Ontology (GO) term mapping of biological processes linked to the MGs suggested that 30.43% of MGs identified in CD4$^+$ T cell subsets encode metabolic processes (GO:0008152), while 31.52% and 1.09% encode cellular processes (GO:0009987) and immune responses (GO:0002376), respectively (Figure 1C).

Reporter metabolites of specific lipids and amino acids are altered during activation of human CD4$^+$ T cells

Reporter metabolite (RM) analysis is an approach for the identification of metabolites in a metabolic network, around which significant transcriptional changes occur (Cakir et al., 2006; Patil and Nielsen, 2005). RM analysis can predict hotspots in a metabolic network that are altered between two different conditions, in this case, Th0 versus Thp cells.

The RM analysis suggests that biosynthetic intermediates of glycolysis and the tricarboxylic acid (TCA) cycle are altered upon CD4$^+$ T cell activation (Figure 2A). RMs such as acetyl-CoA (p.adj = 0.02), oxaloacetate (OAA) (p.adj = 0.01), itaconate (p.adj = 0.04), and itaconyl-CoA (p.adj = 0.04) were upregulated, while citrate (p.adj = 0.02) and fumarate (p.adj = 0.01) were downregulated in Th0 cells as compared to Thp cells. This implies that, upon activation of CD4$^+$ T cells, citrate can be diverted from the TCA cycle to form itaconate via aconitate. This phenomenon has been observed previously in macrophages (Ryan and O'Neill, 2017), where itaconate is upregulated under inflammatory conditions to promote an anti-inflammatory response. However, it remains to be elucidated whether itaconate accumulation during T cell receptor (TCR) activation plays a significant role in metabolic reprogramming (Hooftman and O'Neill, 2019) of T cells.

RMs of amino acids (valine, p.adj = 0.03; cystine, p.adj = 0.007; leucine, p.adj = 0.03; isoleucine, p.adj = 0.03; tyrosine, p.adj = 0.03; phenylalanine, p.adj = 0.01; and threonine, p.adj = 0.01) and glycerophospholipids (phosphatidylcholine [PC] [p.adj = 0.008]) and phosphatidylethanolamine [PE]
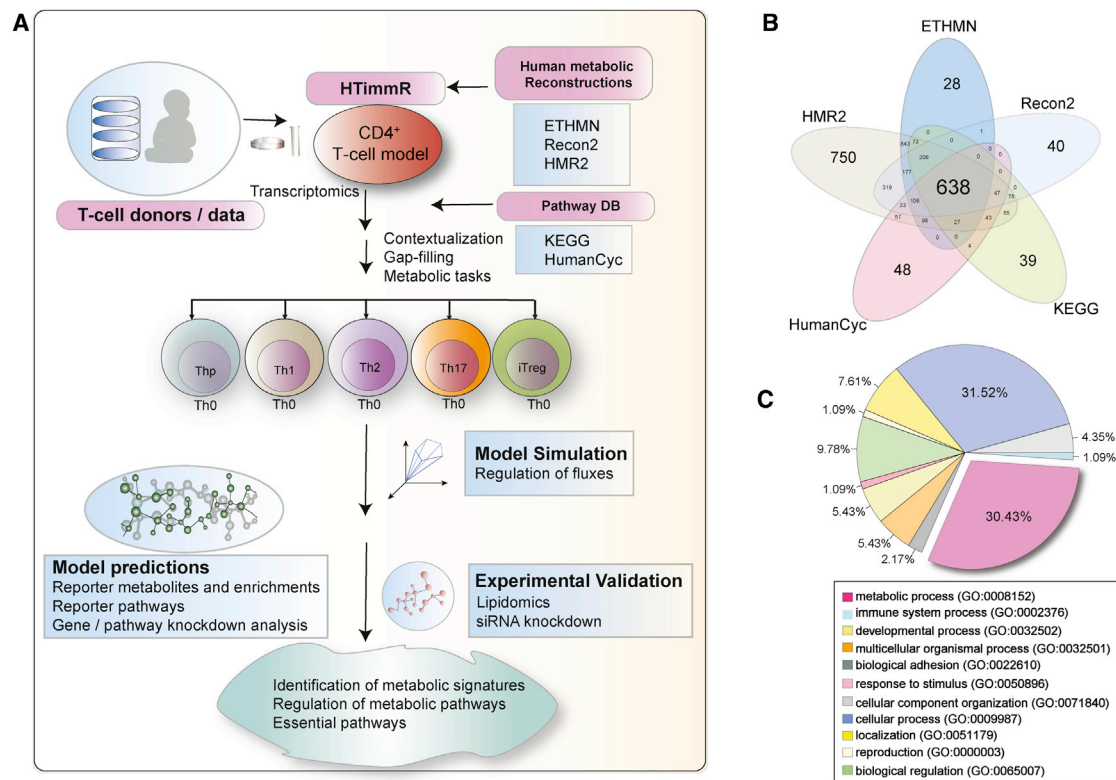
Figure 1. Metabolic reconstruction of human CD4⁺ T cell subsets

(A) Schematic representation showing metabolic reconstruction of generic CD4⁺ T cells (HTimmR), and contextualization of HTimmR to functional genome-scale models (GEMs) for T-naive (Thp), T-activated (Th0), and differentiated T helper (Th) subsets, using lineage-specific gene expression datasets.

(B) Venn diagram showing metabolic genes (MGs) of human CD4⁺ T cells identified in this study, which were commonly or uniquely found in various human metabolic reconstructions (HMR2, ETHMN, RECON) and pathway databases (KEGG and humanCyc).

(C) Pie chart showing the Gene Ontology (GO term) mapping of several biological processes exhibited by the MGs of the CD4⁺ T cells.

[p.adj = 0.008]) were upregulated in Th0 cells as compared to Thp cells (Figure 2A).

Intriguingly, several intermediates of sphingolipids, particularly GSL pathways such as lactosylceramides (LacCers) (p.adj = 0.01) and D-galactosyl-*N*-acylsphingosine (p.adj = 0.03), were downregulated in Th0 cells as compared to Thp cells (Figure 2A).

Overrepresentation analysis of the RM pathways showed that, primarily, lipid (glycerophospholipids and GSLs) and amino acid metabolism were altered (hypergeometric test, q < 0.05) upon CD4⁺ T cell activation (Figure S2).

Differentiation of human CD4⁺ T cell subsets depicts regulation of unique metabolic pathways

RMs of Th1, Th2, Th17, and iTreg cells were identified at 72 h of polarization (Figure 2A). In Th1 cells, we observed that RM pools of NADP⁺ (p.adj = 0.004) and NADPH (p.adj = 0.01) were upregulated as compared to Th0 cells. Differentiation of Th1 cells may alter intracellular levels of oxidative stress, as suggested by the downregulation of peroxisomal glutathione (GSH) (p.adj = 0.01) and H_2O_2 (p.adj = 0.009). Prostaglandins and leukotrienes (12-dehydro-leukotriene B4 and 12-oxo-leukotriene B3) were also downregulated (p.adj = 0.017) (Figure 2A). Overrepresentation analysis of RM pathways suggests that prostaglandin biosyn-

thesis, aromatic amino acid, estrogen, fructose, and mannose metabolism are altered (hypergeometric test, q < 0.05) in the Th1 cells as compared to Th0 cells (Figure 2B).

In Th2 cells, mitochondrial fatty acyl-CoA, including myristoyl-CoA (p.adj = 0.002) and palmitoyl-CoA (p.adj = 0.005) RMs were upregulated as compared to Th0 cells. Intriguingly, these activated fatty acyl-CoAs might induce fatty acid oxidation (FAO) and degradation. Alternatively, cytosolic malonyl-CoA (p.adj = 0.04) was elevated in Th2 cells. Malonyl-CoA inhibits the rate-limiting step of FAO, i.e., transport of FAs to mitochondria via the carnitine shuttle. Our results suggest that there might be a trade-off between fatty acid synthesis (FAS) and FAO that underpins the functional differentiation of Th2 cells (Figure 2A). Several RM pathways such as β-oxidation of unsaturated fatty acids, alanine, aspartate, glutamate, and histidine metabolism, and the pentose phosphate pathway (PPP), GSL, and nucleotide metabolism were altered (hypergeometric test, q < 0.05) in Th2 cells as compared to Th0 cells (Figure 2C).

RM analysis of Th17 showed a markedly different pattern of regulation as compared to Th1 and Th2 cells. Several classes of GSLs (cerebrosides, gangliosides [GMs], *N*-acetylneuraminic acid [NANA]) were upregulated (p.adj < 0.05) in the differentiated CD4⁺ Th17 cells as compared to Th0 cells at 72 h. In addition,
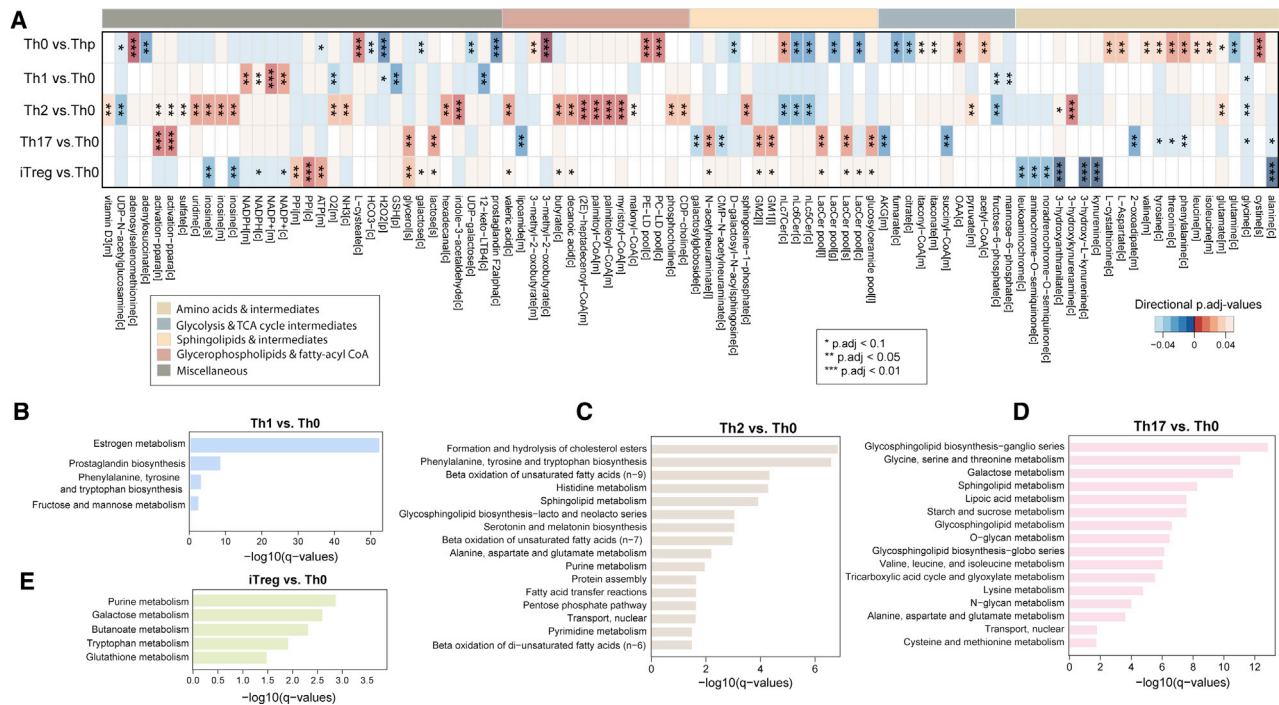
Figure 2. Reporter metabolites and overrepresented pathways of CD4+ T cell activation and differentiation at 72 h of polarization

(A) Heatmap of reporter metabolites (RMs) that are significantly (p.adj < 0.05) upregulated (red) or downregulated (blue) or remained unchanged (white) in the CD4+ T cell subsets as compared to their paired control (Th0 cells). The RMs were grouped by their metabolic subsystems/pathways and marked by the color bars. *p < 0.05, **p < 0.01, ***p < 0.001.

(B–E) Bar plots showing overrepresented (q < 0.05) reporter pathways (RPs) of the CD4+ T cell subsets.

some of the aromatic amino acids were downregulated (p.adj < 0.05) (Figure 2A). Overrepresentation analysis of RM pathways showed that sphingolipids, particularly GSL, amino acid metabolism, and other related metabolic processes were altered (hypergeometric test, q < 0.05) in Th17 cells as compared to Th0 cells (Figure 2D). Notably, GSLs (LacCers, GMs, and NANA) were found to be a unique signature of differentiated CD4+ Th17 cells as compared to Th1 and Th2 cells. Some of these GSLs displayed a similar trend in the iTreg versus Th0 cells, but the changes did not reach statistical significance (p.adj = 0.09). Additionally, RMs of the tryptophan/kynurenine pathways, i.e., kynurenine, 3-hydroxyanthranilate, formylanthranilate, and quinones, were downregulated (p.adj = 0.0008) (Figure 2A). Of note, tryptophan is metabolized to kynurenine by indoleamine 2,3-dioxygenase, an enzyme that is induced by pro-inflammatory cytokines (Dantzer, 2017). In addition, several short- and long-chain fatty acids such as butyric (p.adj = 0.06), decanoic (p.adj = 0.06), and valeric (p.adj = 0.06) acids were upregulated in the iTreg versus Th0 cells. Overrepresentation analysis of RM pathways showed that tryptophan, glutathione, butanoate, galactose, and purine metabolism were overrepresented in iTreg cells as compared to Th0 cells (Figure 2E).

Dynamic regulation of molecular lipids in human CD4+ T cell subsets

Taken together, RM analysis of CD4+ T cell activation and differentiation predicted several classes of metabolites and pathways

as being altered between the various subsets (Figure 2; Figures S2–S4). RMs of lipids and amino acids were found to be the predominant classes significantly altered in CD4+ T cells during activation and at 72 h of differentiation. While the importance of amino acids in CD4+ T cell differentiation is well established (Carr et al., 2010; Poffenberger and Jones, 2014), the role of molecular lipids in the differentiation of human CD4+ T cells remains uncharacterized. Furthermore, RMs of glycerophospholipids and GSLs were markedly altered in Th17 and iTreg cells as compared to Th1 and Th2 cells (Figure 2). Thus, the above findings directed us to investigate the dynamics of molecular lipids in CD4+ T cell differentiation.

Naive CD4+ T cells were isolated from individual human umbilical cord blood donors and were TCR activated using anti-CD3 and anti-CD28. By adding different cytokines, naive CD4+ T cells were differentiated into distinct effector T helper (Th1, Th2, and Th17) and iTreg cell subsets, which are characterized by expression of lineage-specific transcriptional regulators, cell surface markers, and secretion of key cytokines. For the control cells (Th0), CD4+ T cells were TCR stimulated with anti-CD3 and anti-CD28 without differentiating cytokines and cultured in parallel. In addition, naive, unstimulated CD4+ T cells were collected from each donor as functional immature Thp cells. Differentiated T helper subsets were characterized by expression of lineage-specific transcriptional regulators, cell surface markers, and secretion of key cytokines. Th1 and Th2 differentiation was characterized by lineage-specific transcription factors T-bet and

GATA3, respectively, using flow cytometry. Polarization of Th17 cells was validated by the expression of the surface chemokine receptor CCR6 and the expression and secretion of Th17 key cytokines IL-17A and IL-17F. As FOXP3 is the master transcription factor regulator in Treg cells, its expression was analyzed in iTreg cells (see STAR Methods).

We profiled the molecular lipids of human CD4+ T cell subsets (n = 5) using the established lipidomics platform, which is based on ultra-high-performance liquid chromatography and quadrupole time-of-flight mass spectrometry (UHPLC-QTOFMS). Sparse partial least-square discriminant analysis (sPLS-DA) (Lê Cao et al., 2011) of the lipidomics dataset reveled that the lipidome of resting naive (Thp) cells was different from the activated or differentiated T cell subsets (R^2X = 0.933, R^2Y = 0.988, N = 7-fold cross-validated Q^2 = 0.886; Figure 3A). Th17 and iTreg cells were different from each other and also from the Th1 and Th2 cells (Figure 3A). Several classes of lipids, such as lysophosphatidylcholines (LPCs), PCs, PEs, sphingomyelins (SMs), ceramides (Cers), and triacylglycerols (TGs) were altered (regression coefficient [RC] > ±0.05 and variable importance in projection [VIP] scores [Farrés et al., 2015] >1) in the CD4+ T cell subsets at 72 h of differentiation (Figure 3B).

To gain statistical confidence in the selection of the lipid markers between two different cell types, we combined two statistical approaches, i.e., multivariate (sPLS-DA, n = 7-fold cross-validation [CV]) and univariate (paired t test). We thereby identified lipids that were significantly altered between CD4+ T cell subsets (n = 5) and their paired Th0 cells (controls) (Figure 3C) (see STAR Methods). We found that PCs, LPCs, SMs, and Cers were altered in the T cell subsets during activation and early differentiation (Figure 3C), consensually determined by two statistical approaches (sPLS-DA: area under the curve [AUC] ~0.85, RC > ±0.05, and VIP scores >1.2, and paired t test, p.adj < 0.05, adjusted for FDR) (see STAR Methods). Most cellular PCs were upregulated in the Th2, Th17, and iTreg cells, while these were downregulated in Th1 cells, as compared to their paired Th0 cells (Figure 3C). Cer(d18:1/16:0), Cer(d18:1/24:1), and dihexosyl ceramide (diHexCer)(d18:1/16:0) were elevated in Th17 and iTreg cells. Mostly, SMs were altered in Th2 and iTreg cells. Some SMs, i.e., SM(d32:1), SM(d36:1), and SM(d42:1), were upregulated in Th17 cells (versus Th0 cells), while they were downregulated in iTreg cells (versus Th0 cells) (Figure 3C). Cellular TGs were markedly elevated in iTreg and Th17 cells (Figure 3C). The lipidome data suggest that glycerophospholipids (PCs, PEs, and LPCs) and sphingolipids (Cers, GSLs, and SMs) are the major indicators of CD4+ T cell differentiation (Figures 3B and 3C).

Dynamic regulation of Cers and GSLs during the early differentiation of human CD4+ Th17 and iTreg cells

GSLs and Cers play an important role in maintaining the integrity of the plasma membrane. They are involved in cellular signaling, proliferation, endocytosis, and modulate cellular responses to inflammatory and apoptotic stress signals (Apostolidis et al., 2016; Zhang et al., 2019). However, the functional role of these metabolites in CD4+ T cell activation and differentiation remains unknown (Zhang et al., 2019). Here, RM predictions and lipidome analysis of human CD4+ T cells have, together, identified several

species of GSLs that were altered in Th17 (versus Th0) and iTreg cells (versus Th0 cells) at 72 h of differentiation (Figures 2A, 3B, and 3C).

Next, by applying RM analysis, we investigated the regulation of GSLs and Cers in Th17 and iTreg cells during the first 48 h of polarization. RM analysis was performed between Th17 versus Th0 cells at 0.5, 1, 2, 4, 6, 12, 24, and 48 h of differentiation. Initially, the RMs of Cers were elevated at 1 h, and subsequently there was a transient decrease at 2 h, followed by an increase at 12, 24, and 48 h of differentiation (Figure S3). A similar pattern of regulation was also observed in ceramide 1-phosphate (C1P), an active intermediate of sphingolipid metabolism (Figure S3).

In iTreg cells, several RMs of the sphingolipid pathway such as digalactosylceramides, D-galactosyl-N-acylsphingosine, UDP-galactose, and di-hexosylceramides (diHexCers), particularly LacCers, were upregulated (versus Th0 cells) by 6 h of polarization (Figure S4). However, no change in the levels of LacCers were observed in Th17 cells at these early time points (Figure S3).

Targeted lipid measurements reveal the regulation of Cer levels in human CD4+ Th17 and iTreg cells at 72 h of differentiation

A targeted lipidomics experiment was designed to measure the levels of Cers and GSLs (i.e., HexCers and diHexCers in human CD4+ Th17 (n = 3) and iTreg cells (n = 5), at 72 h of differentiation (Figure 4; Table S1). Increased levels of Cers, as well as decreased levels of HexCers, were found in both Th17 and iTreg cells, except for HexCer(18:1/24:0), which was elevated (p = 0.04) in iTreg cells (Figure 4H). Intriguingly, diHexCers (d18:1/16:0) were elevated in Th17 versus Th0 cells (p = 0.001), while these changes were not apparent (p > 0.05) in iTreg versus Th0 cells (Figure 4I).

There was congruence between the results obtained from GSMM-RM predictions (Figure 2A) and from non-targeted (Figures 3B and 3C) and targeted (Figure 4) lipidomics measurements showing that GSLs (specifically Cers and diHexCers) were elevated in CD4+ Th17 cells (p < 0.05).

Relative contribution of the sphingolipid pathways to the production of Cers in Th17 cells

We evaluated the effect of various metabolic reactions of the sphingolipid pathway on Cer production in CD4+ Th17 cells at 72 h of differentiation (Figure 5A). An in silico knockout (KO) analysis of Th17 cells was performed using GSMM, where each reaction of the sphingolipid pathway was knocked out iteratively, one at a time, and the percentages of maximum flux contributions for Cer production via different neighboring reactions (NRs) were estimated (Figures 5A and 5B) (see STAR Methods). Optimization of Cer production in a wild-type (WT) model (no KOs) suggests that ~30% of the total flux of Cer production can be carried by de novo synthesis, i.e., by conversion of dihydroceramide to Cer (Figures 5A and 5B). As expected, by knocking out serine palmitoyltransferase (SPT), a rate-limiting step in the de novo sphingolipid synthesis pathway (Hanada, 2003), decreased the total flux of Cer production; however, it could not completely abolish the Cer production (Figure 5B). This is due to the presence of redundant sphingolipid reactions that replenish Cers in Th17 cells (Figures 5A and 5B).
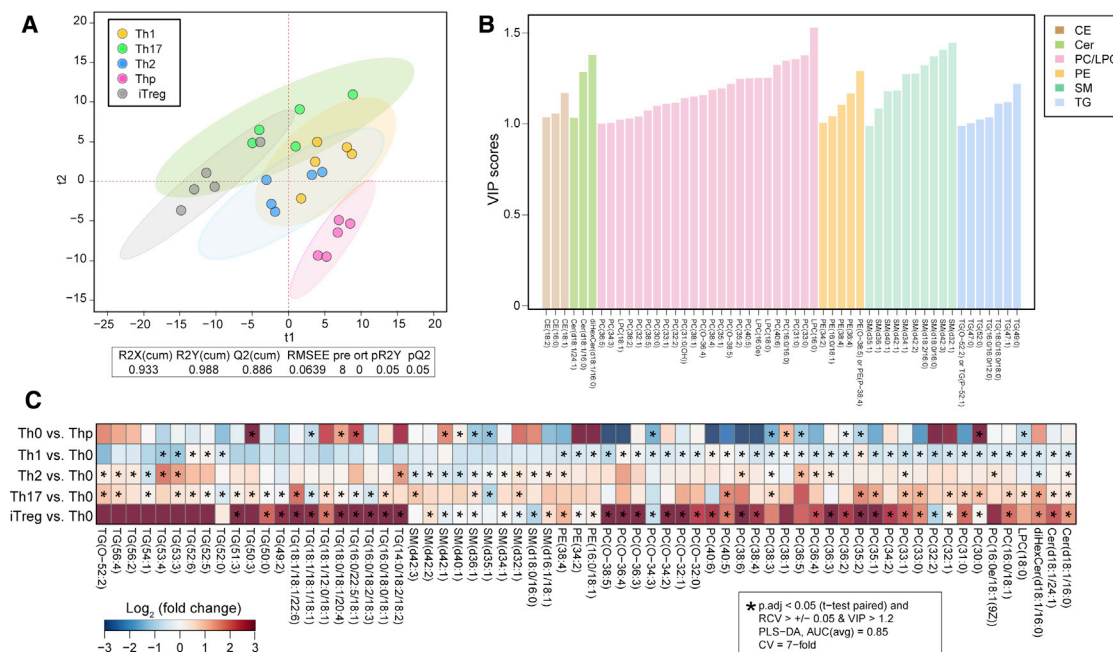
Figure 3. Lipidome of human CD4⁺ T cell activation and differentiation

(A) Scatterplot/score plot for the PLS-DA classification model (model performance: $R^2X = 0.933$, $R^2Y = 0.988$, N = 7-fold cross-validated (CV), $Q^2 = 0.886$), showing differences in the lipidomes of the T cell subsets, isolated from the umbilical cord of (n = 5) healthy neonates. Ellipse denotes 95% confidence region.

(B) Bar plot showing VIP scores of the lipids included in the PLS-DA classification model. The lipids are grouped and color coded by their chemical classes. Different classes of lipids such as cholesterol esters (CEs), phosphatidylcholines (PCs), lysophosphatidylcholines (LPCs), phosphatidylethanolamines (PEs), sphingomyelins (SMs), ceramides (Cers), dihexosyl ceramides (diHexCers), and triacylglycerols (TGs) with (VIP scores > 1) are shown.

(C) Heatmap showing $\log_2$ fold changes (FCs) of the significantly altered lipids between T cell subsets versus Th0 cells at 72 h of polarization. Red denotes increase while blue denotes decrease; white denotes no change. *p < 0.05, significant difference in the levels of the lipids as determined by univariate (paired t test, p.adj < 0.05) and multivariate (PLS-DA; abs(RCV) > 0.05 and VIP > 1.2) analyses.

Effects of *SPTLC1,2,3* silencing on Cer levels in human CD4⁺ Th17 cells

De novo biosynthesis of Cer starts with the *SPT* pathway, a rate-limiting step that aids in the condensation of serine and palmitoyl-CoA by an enzyme complex called serine palmitoyl transferase (*SPTLC*) (Figures 5A and 6A). Currently, there are three major *SPTLC* subunits identified, including *SPTLC1*, *SPTLC2*, and *SPTLC3*, which are known to be expressed in humans (Hornemann et al., 2009).

Based on our RNA sequencing (RNA-seq) data, the three *SPTLC* subunits are expressed during human Th17 cell differentiation (Figure S5). To examine changes in Cer biosynthesis during Th17 cell development, we simultaneously silenced these three SPTLC subunits (*SPTLC1,2,3* triple knockdown [TKD]) using small interfering RNAs (siRNAs). As illustrated in Figures 6B–6E, the three siRNAs successfully downregulated their targets. Importantly, silencing of *SPTLC* decreased the expression of the proinflammatory cytokines IL-17A (p = 0.08) and IL-17F (p = 0.001) in Th17 cells at 72 h following cell activation (Figures 6F and 6G), suggesting that Cer synthesis is vital for Th17 cell function.

Similarly, through a mass spectrometry-based targeted lipidomics experiment, we measured the Cer levels in these Th17 (TKD) cells at 72 h of polarization. Several species of Cers and GSLs (HexCers, diHexCers) were significantly decreased in

SPTLC-deficient Th17 cells (Figures 6H–6P). Most importantly, diHexCers levels were significantly reduced upon *SPTLC* silencing, suggesting that regulation of diHexCers is associated with the Th17 differentiation and effector function (Figures 6N–6P). Overall, these results suggest that silencing of the three *SPTLC* subunits negatively influences the development and secretory function of human CD4⁺ Th17 cells (Figures 6F and 6G).

Effect of *UGCG* silencing on HexCer and LacCer synthesis in human CD4⁺ Th17 cells

diHexCers (LacCers) can be generated from HexCers (GlcCers), which, in turn, are produced from Cers and glucose, catalyzed by glucosylceramide synthase (GCS) (EC 2.4.1.80), encoded by the *UGCG* gene. This is the first committed step in the production of GlcCer-related GSLs (Alam et al., 2015) (Figures 5A, 7A, and 7D). Results from the *SPTLC* gene silencing experiment in Th17 cells showed an effective downregulation of diHexCers (Figures 6N–6P). Furthermore, these findings guided us to evaluate the importance of the GCS pathway for the production of GlcCers and diHexCers in human CD4⁺ Th17 cells.

Similarly, by taking a siRNA-mediated silencing approach, we knocked down expression of the *UGCG* gene (Figure 7B), which encodes GCS in Th17 cells (Figure S5). Although expression of the IL-17 cytokine was not influenced by *UGCG* knockdown in
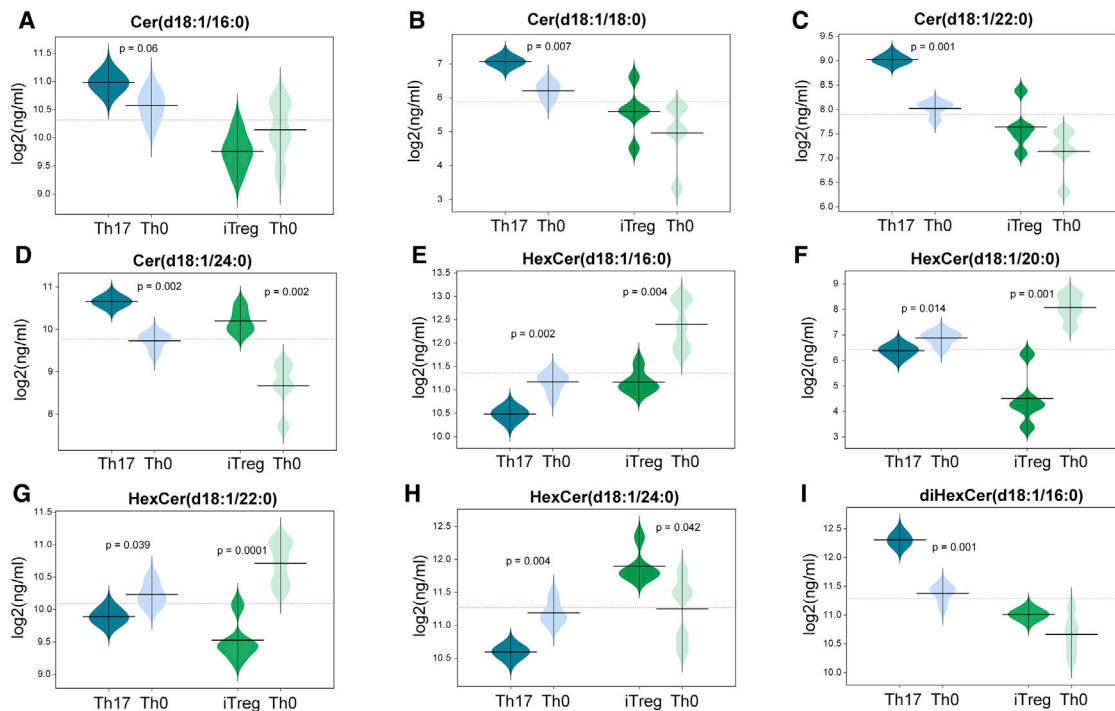
Figure 4. Targeted quantification of ceramide levels in Th17 and iTreg cells

(A and D) Bean plots showing ceramide levels (log$_2$ [ng/mL]) measured in Th17 and iTreg cells differentiated from CD4$^+$ T cells isolated from the umbilical cord of healthy neonates (n = 5) and their paired controls (Th0) at 72 h of polarization.

(E–I) Cellular levels of HexCers and diHexCers in the Th17 and iTreg cells along with their paired controls (Th0), at 72 h of polarization. Significant differences (paired t test, p < 0.05) are shown by the p values. The dotted line denotes the mean of the population, and the black dashed lines in the bean plots represent the group mean.

Th17 cells, we decided to determine changes in the production of HexCers, diHexCers, and SMs in *UGCG*-deficient Th17 cells. As expected, several species of Cers, HexCers (GlcCers and/or GalCers), and diHexCers (except diHexCer(d18:1/16:0)) were decreased in the *UGCG*-silenced Th17 cells (Figure 7C). A decrease in Cer levels implies that Cer can be diverted to other sphingolipid pathways (*CerS, SMS, C1PP*; Figure 5A), and thus might enhance the production of sphingosines, SMs, and ceramide 1-phosphate, respectively. Intriguingly, several species of SMs were elevated in the *UGCG*-silenced Th17 cells, suggesting that production of SMs via the SMS-pathway was enhanced with a pertinent decrease in Cers and GSLs (Figure 5A; Figure S5).

Cer pathways were altered in the immune cells of children who progressed to islet autoimmunity and type 1 diabetes later in life

Next, we examined potential relevance of our findings to the understanding of lipid-related pathways in the development of type 1 diabetes (T1D). Our previous lipidomics study suggests that T1D is preceded by specific alteration of lipids in PBMCs from children who progressed to islet autoimmunity or overt T1D later in life (Sen et al., 2020). Here, we investigated whether sphingolipids and their metabolic pathways are altered in the immune cells with the appearance of β cell autoantibodies and/or overt

clinical T1D. By using GSMM together with the published "multi-omics" datasets we studied the regulation of sphingolipid metabolism in CD4$^+$ T cells and PBMCs of the children who developed β cell autoimmunity (cases) and/or progressed to clinical T1D (cases), as compared to the healthy controls (HCs) from two perspective cohorts (Kallionpää et al., 2019; Sen et al., 2020).

Differential expression analysis of MGs showed that the *SPTLC3* gene, encoding the *de novo SPT* pathway (Figures 5 and 6A), was upregulated (p.adj < 0.05, adjusted for FDR) in the CD4$^+$ T cells and PBMCs of the children who develop β cell autoimmunity (>1 islet autoantibodies) versus HCs (Figure S6). These changes were apparent in all the cases at 24 months of age, i.e., after seroconversion (median age ± SD of 18 ± 4.5 months) (Kallionpää et al., 2019) (Figure S6). At that age, the expression levels of *CERS6* and *SGMS1,2* that facilitate Cer and SM production, respectively, were also elevated in the CD4$^+$ T cells of the cases (versus HCs) (Figure 5A; Figure S6). Additionally, the *GBA* gene that facilitates Cer production from HexCers (GlcCers) via the β-glucocerebrosidase (GCDase) pathway was elevated (p.adj < 0.05) in the CD4$^+$ T cells and PBMCs of the cases versus HCs at 18 months of age (Figure 5A; Figure S6). Intriguingly, the expression of these genes was markedly (p.adj < 0.05) decreased in the cases (versus HCs) at 36 months of age (Figure S6).
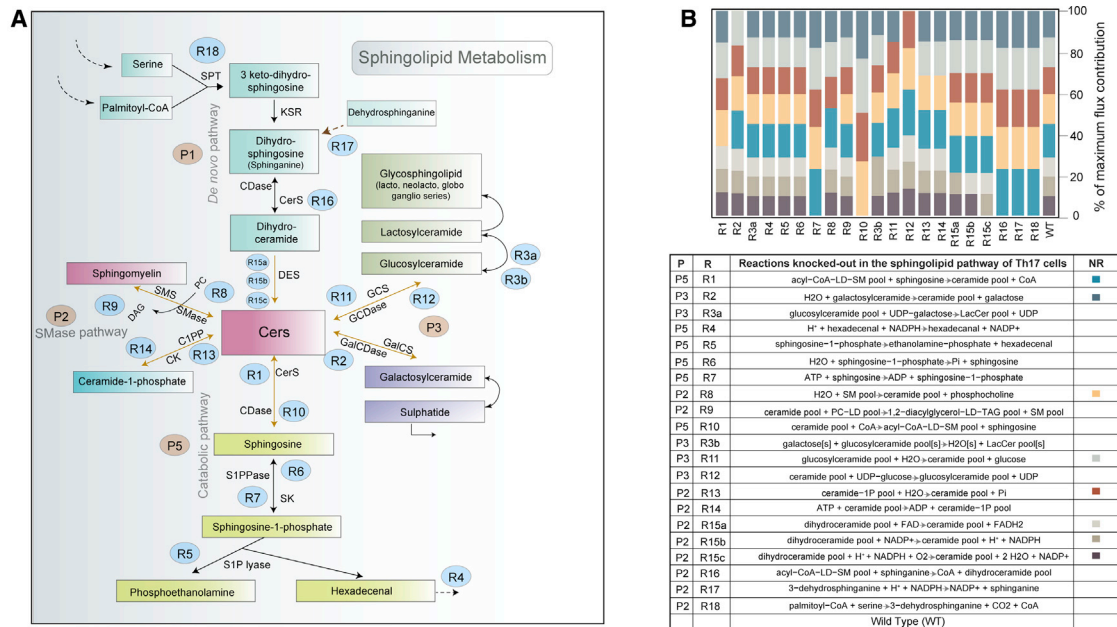
Figure 5. Regulation of sphingolipid pathways in human CD4+ T cells

(A) Illustration of sphingolipid metabolism in human CD4+ T cells. R# and P# denote reaction and pathway identifiers, respectively. A reaction involving different co-factors was optimized separately. The identifiers of these reactions are prefixed with letters. Neighboring reactions (NRs) that were maximized (objective function) and contributed directly toward Cer production are marked with yellow arrows.

(B) In silico knockout (KO) analysis showing the % of "maximized" fluxes of different NRs by in silico knockout (one-by-one) of an alternate reaction of the sphingolipid pathway.

C1P, ceramide 1-phosphate; CDase, ceramidase; CerS, ceramide synthase; DES, dihydroceramide desaturase; GalCDase, galactosidase; GCDase, glucosidase; S1P; sphingosine 1-phosphate; S1PPase, sphingosine phosphate phosphatase; SK, sphingosine kinase; SMase, sphingomyelinase pathway; SPT, serine palmitoyl-CoA transferase.

P	R	Reactions knocked-out in the sphingolipid pathway of Th17 cells	NR
P5	R1	acyl–CoA–LD–SM pool + sphingosine ⇒ceramide pool + CoA	■
P3	R2	H2O + galactosylceramide ⇒ceramide pool + galactose	■
P3	R3a	glucosylceramide pool + UDP–galactose⇒LacCer pool + UDP	
P5	R4	H⁺ + hexadecenal + NADPH⇒hexadecenal + NADP+	
P5	R5	sphingosine–1–phosphate⇒ethanolamine–phosphate + hexadecenal	
P5	R6	H2O + sphingosine–1–phosphate⇒Pi + sphingosine	
P5	R7	ATP + sphingosine⇒ADP + sphingosine–1–phosphate	
P2	R8	H2O + SM pool⇒ceramide pool + phosphocholine	■
P2	R9	ceramide pool + PC–LD pool⇒1,2–diacylglycerol–LD–TAG pool + SM pool	
P5	R10	ceramide pool + CoA⇒acyl–CoA–LD–SM pool + sphingosine	
P3	R3b	galactose[s] + glucosylceramide pool[s]⇒H2O[s] + LacCer pool[s]	
P3	R11	glucosylceramide pool + H2O⇒ceramide pool + glucose	■
P3	R12	ceramide pool + UDP–glucose⇒glucosylceramide pool + UDP	
P2	R13	ceramide–1P pool + H2O⇒ceramide pool + Pi	■
P2	R14	ATP + ceramide pool⇒ADP + ceramide–1P pool	
P2	R15a	dihydroceramide pool + FAD⇒ceramide pool + FADH2	■
P2	R15b	dihydroceramide pool + NADP+⇒ceramide pool + H⁺ + NADPH	■
P2	R15c	dihydroceramide pool + H⁺ NADPH + O2⇒ceramide pool + 2 H2O + NADP+	■
P2	R16	acyl–CoA–LD–SM pool + sphinganine⇒CoA + dihydroceramide pool	
P2	R17	3–dehydrosphinganine + H⁺ + NADPH⇒NADP+ + sphinganine	
P2	R18	palmitoyl–CoA + serine⇒3–dehydrosphinganine + CO2 + CoA	
		Wild Type (WT)	

By using the gene expression datasets, we developed cell-type functional GEMs for CD4+ T cells and PBMCs (see STAR Methods). GSMM of these cells showed that there is an overall (at all time points) increase in the average flux of sphingolipid pathways in the CD4+ T cells of the children who develop β cell autoimmunity versus HCs (Figure S7). The key pathway changes were observed around SM, LacCer, and dihydroceramide pools (Figure 5A; Figure S7).

To validate the intracellular levels of Cers in the development of β cell autoimmunity and/or clinical T1D, we extended our analysis to another longitudinal T1D cohort (Sen et al., 2020). Here, we expanded the panel of sphingolipids previously measured in the PBMCs (Sen et al., 2020) obtained from the children who developed β cell autoimmunity (≥1 islet autoantibodies) without progressing to T1D (P1Ab, n = 27) or later progressed to clinical T1D (PT1D, n = 34), as well as HCs (seronegative) (n = 10) (Sen et al., 2020). Differential analysis between the cases (P1Ab or PT1D) versus HCs showed an increase in the intracellular levels of Cers at 24 months of age; the effect was more prominent in the P1Ab (versus HC) group. Of note, some of these Cers were elevated (p.adj < 0.05) in Th17 (versus Th0) and/or iTreg (versus Th0) cells but not in Th1 and Th2 cells at 72 h of polarization (Figures 3 and 4; Figure S7). At 36 months of age, several molecular species of Cers such as Cer(d44:2), Cers(d18:1/20-25), Cer(d36:1), Cer(d40:1), and Cer(d42:1), as well as SM(d18:1/24:0), were downregulated (p.adj < 0.05) in PT1D versus HC groups (Figure S7).

DISCUSSION

We showed that human CD4+ T cell subsets, i.e., Th1, Th2, Th17, and iTreg cells, undergo both common and subset-specific metabolic alterations in order to both successfully differentiate and subsequently carry out their specific functions. RM analysis suggests that, upon the activation of naive T cells, the levels of the amino acids increase, while most of these amino acids then decrease toward a Treg cell phenotype. Indeed, iTreg cells are thought to be less dependent on amino acids (Newton et al., 2016). For instance, depletion of glutamine can skew the differentiation of CD4+ T cells toward a Treg cell lineage (Klysz et al., 2015).

Cers are key intermediates of sphingolipid metabolism, composed of a sphingosine base and a fatty acyl chain (C14:0–C26:0) (Gault et al., 2010). Cers are important for T cell activation and differentiation at multiple levels, such as intracellular signal transduction, modulation of membrane fluidity, receptor clustering, and by contributing to CD95-mediated cell death via multiple mechanisms (Adam et al., 2002). However, the Cer pathways are highly redundant. One of the key novel observations from our RM and lipidomics analyses was that several species of Cers and GSLs are markedly altered in Th17 and iTreg cells at 72 h of differentiation. The observed alterations in the levels of Cers and GSLs (HexCers, diHexCers) were prominent in Th17 cells as compared to iTreg cells. diHexCers (LacCers) were markedly high in the differentiated Th17 versus Th0 cells.
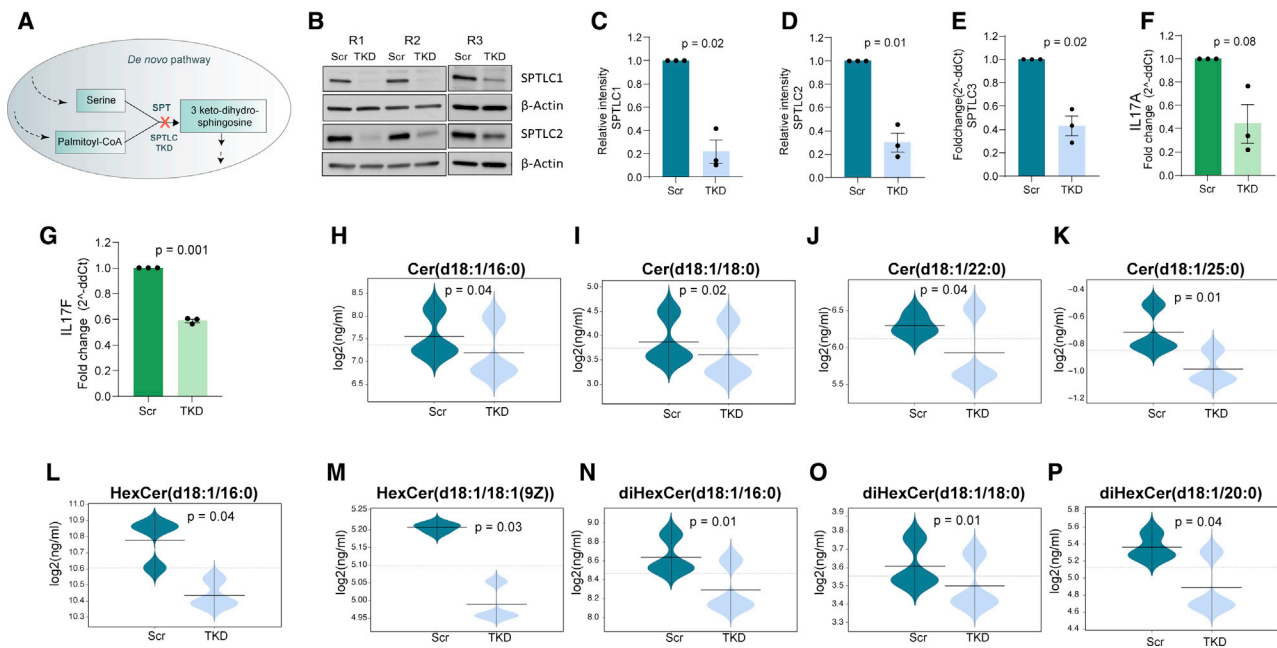
Figure 6. Effect of *SPTLC* deficiency on the serine palmitoyltransferase (SPT) *de novo* pathway and Th17 differentiation

(A) Illustration of *SPT* (*SPTLC*) TKD.

(B–E) Immunoblots and corresponding quantified intensities of *SPTLC1* and SPTLC2 protein expression at 24 h and fold changes of *SPTLC3* mRNA expression by quantitative real-time PCR (TaqMan) at 72 h upon *SPTLC* TKD in Th17 cell differentiation (Scr versus *SPTLC* TKD; n = 3; paired t test, p < 0.05).

(F and G) Fold changes of IL-17A and IL-17F mRNA expression by quantitative real-time PCR (Scr versus *SPTLC* TKD) at 72 h of Th17 cell differentiation (n = 3; paired t test, p < 0.05).

(H–P) Bean plots showing the targeted quantification levels of (log$_2$ [ng/mL]) Cers, HexCers, and diHexCers measured in control (Scr) and *SPTLC*-deficient Th17 cells at 72 h (n = 3). Significant differences (paired t test, p < 0.05) are shown by the p values. The dotted line denotes the mean of the population, and the black dashed lines in the bean plots represent the group mean.

Furthermore, *in* vitro knockdown experiments substantiated the essentiality of sphingolipid metabolic pathways (*SPT*, *GCS*) in the formation of Cers and GlcCers/diHexCers, and these are intrinsically linked to proinflammatory cytokine (IL-17A and IL-17F) expression in Th17 cells. Several species of diHexCers were decreased in the knockdowns, suggesting that accumulation of diHexCers is required for Th17 cell differentiation. In addition, RM analysis of Th17 cells showed a persistent increase in the Cer pool from 12 h until 72 h of polarization.

An earlier study observed accumulation of Cers in Treg cells as a consequence of low sphingomyelin synthase *SMS1* (encoded by *Sgms1*), an enzyme catalyzing the conversion of Cers and PCs to diacylglycerols and SMs (Apostolidis et al., 2016). In line with this, several species of SMs measured in our study were shown to be decreased in the iTreg versus Th0 cells, and increased in Th17 versus Th0 cells, while few SMs (SM(d16:1/18:1) and SM(d42:3)) were elevated in both iTreg and Th17 cells (Figure 3C). In Treg cells, FOXP3 directly binds to *Sgms1* to suppress *SMS1,* and retroviral overexpression of FOXP3 in Jurkat human T lymphocytes decreased the expression of *SGMS1* (Apostolidis et al., 2016; Arvey et al., 2014). The accumulation of Cers constrains *SET* activity toward protein phosphatase A (*PP2A*). Intriguingly, *PP2A* can suppress mTORC1 activity and promotes Treg and Th17 cell differentiation (Apostolidis et al., 2013, 2016; Xu et al., 2019)

Furthermore, several studies indicate that co-expression of CD39 (*ENTPD1*) and CD161 (*KLRB*) in Th17 cells increases the activity of acid sphingomyelinase (*ASM*), an enzyme encoded by the gene *SMPD1*, which hydrolyzes SMs to form Cers and phosphorylcholine, in turn leading to an increase in the Cer pool (Bai and Guo, 2017; Bai et al., 2014; Bai and Robson, 2015). Although *ENTPD1* levels remain unchanged during the early differentiation of iTreg and Th17 cells, *KLRB* is specifically downregulated in Th17 cells (Tuomela et al., 2016; Ubaid Ullah et al., 2018). Furthermore, *SMPD1* is upregulated in iTreg cells (Ubaid Ullah et al., 2018), suggesting intrinsic regulation of Cers in both Th17 and iTreg cells.

We found specific regulation of the sphingolipid pathways in the CD4$^+$ T cells and PBMCs associated with the development of β cell autoimmunity and progression to T1D. T1D is characterized by a T cell-mediated autoimmune destruction of the pancreatic β cells in genetically predisposed individuals (Atkinson, 2014; Eisenbarth, 1986). Our previous lipidomics studies suggest that T1D is preceded by specific disturbances in the lipid metabolism, including dysregulation of sphingolipid metabolism in the PBMCs (Sen et al., 2020). Recently, in a longitudinal cohort setting, Kallionpää et al. (2019) showed that several genes were differentially regulated in the CD4$^+$ T cell fractions, as well as unfractionated PBMCs, collected from children who developed β cell autoimmunity versus the HCs. By performing integrative
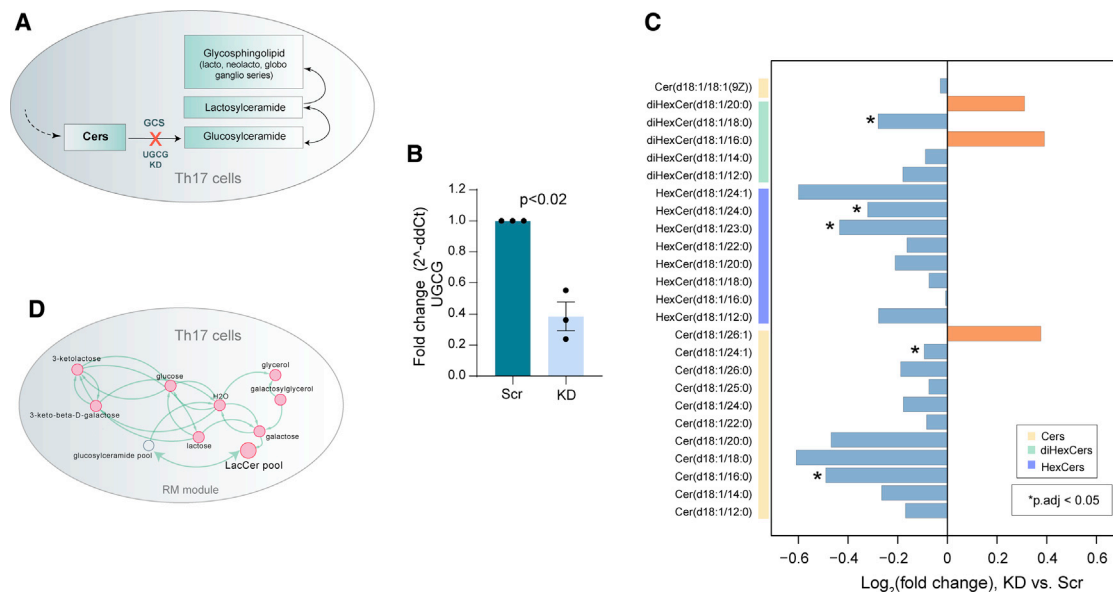
Figure 7. Targeted quantification of the Cer and GSL levels in the *UGCG*-deficient Th17 cells

(A) Illustration of the GCS pathway and *UGCG* knockdown.

(B) Fold change of *UGCG* gene expression determined by quantitative real-time PCR, in control (Scr) and *UGCG*-deficient Th17 cells at 12 h (n = 3; paired t test, p < 0.05).

(C) Bar plot showing $\log_2$ fold changes of the Cers, HexCers, and diHexCers measured in *UGCG*-deficient (KD) versus control (Scr) Th17 cells at 72 h (n = 3).

(D) Elevated RM pathway module (p < 0.05) comprising GlcCers, diHexCers, and their congeners in Th17 cells, identified in this study.

analysis of two longitudinal T1D cohorts (Kallionpää et al., 2019; Sen et al., 2020), we found that expression of MGs and predicted fluxes of sphingolipid pathways were altered in the CD4+ T cells and PBMCs after seroconversion, or at the onset of clinical T1D. There was an increase in the expression of MGs and predicted fluxes across the Cer pathways in CD4+ T cells of the children with the appearance of multiple (>1) β cell autoantibodies (24 months, after seroconversion). These might be facilitated by *de novo SPT* (*SPTLC3*), *CerS* (*CerS5*), and *SMS* (*SGMS*) pathways. At that age, accumulation of several molecular species of Cers(d18:1/20–25) that were identified in the PBMCs of the children progressed to clinical T1D (versus HCs). In our study, Cers(d18:1/20–25) were found to be accumulated in Th17 (versus Th0) and iTreg (versus Th0) cells at 72 h of polarization. Furthermore, *in vitro* knockdown experiments have substantiated the importance of Cers in the proinflammatory cytokine expression of CD4+ Th17 cells. Furthermore, no such changes were marked in the Th1 (versus Th0) and Th2 cells (versus Th0 cells).

When examining the sphingolipid pathways in immune cells of children who progressed to islet autoimmunity and clinical T1D later in life, based on data from previous studies (Kallionpää et al., 2019; Sen et al., 2020), we found them markedly changed. For example, the *de novo SPT* pathway (*SPTLC3* gene) was altered in the CD4+ T cells (cases versus HCs). Since in the present study we have demonstrated the essentiality of Cers and GSL synthesis pathways for Th17 differentiation and effector function, our findings may suggest the impact of Cer pathways in CD4+ T cell activation, differentiation, and effector functions in the pathogenesis of T1D. To this end, our study identified

several common and subset-specific metabolic signatures and pathways in human CD4+ T cells for their activation and functional differentiation. This enabled us to improve understanding of how molecular lipids are regulated in different subsets of CD4+ T cells. The study may, therefore, provide a comprehensive resource for identifying CD4+ T cell-specific metabolic pathways and useful targets for their selective manipulation under disease conditions characterized by an imbalance of Th17/natural Treg (nTreg) cells (Chang and Pearce, 2016; O'Sullivan and Pearce, 2015; Sen et al., 2020; Sugiura and Rathmell, 2018).

Our study may also offer clues about the poorly understood overlap in co-morbidities between these immune-mediated diseases and metabolic diseases, such as has been found to occur in coronavirus disease 2019 (COVID-19) (Sattar et al., 2020). Obesity is commonly associated with chronic elevation of circulating fatty acids, which results in the accumulation of, among others, toxic lipids, such as Cers, in peripheral cells/tissues, a phenomenon referred to as lipotoxicity (Virtue and Vidal-Puig, 2010). The presence of elevated levels of Cers in conditions such as obesity and insulin resistance may thus skew the Th17/nTreg balance toward the pro-inflammatory Th17 phenotype, which is also being reported as one of the notable hallmarks of severe COVID-19 (Wang et al., 2020; Wu and Yang, 2020).

Limitations of study

Our study unveiled the importance of Cers and the *de novo* sphingolipid pathway in functional differentiation and effector function of CD4+ T cell subsets, particularly Th17 cells. As a limitation, only subtle phenotypic changes were observed by

knocking down specific MGs of GSL pathways, which may be due to the partial knockdowns of these targets by siRNA. In order to enhance and substantiate the effect of specific gene deletions on CD4$^+$ T cells, mechanistic CRISPR-Cas9 knockout experiments will need to be performed in the future. Fluxomics studies are also needed to deconvolute the regulation of sphingolipid pathways in CD4$^+$ T cell subsets under aberrant conditions. GEMs constrained with experimental fluxes may improve the accuracy of prediction of phenotypes. It also remains to be established how sphingolipid pathways are regulated in autoimmune disease, and whether manipulating these pathways can inhibit an excessive immune response, which, in turn, might suppress the onset of autoimmune disease such as T1D.

STAR★METHODS

Detailed methods are provided in the online version of this paper and include the following:

- KEY RESOURCES TABLE
- RESOURCE AVAILABILITY
  - Lead contact
  - Materials availability
  - Data and code availability
- EXPERIMENTAL MODEL AND SUBJECT DETAILS
  - Human experiments
- METHOD DETAILS
  - Human CD4$^+$ T cell isolation, activation, and differentiation
  - siRNA-mediated gene knockdown
  - Western blot
  - Quantitative real-time PCR
  - Analysis of molecular lipids
  - Measurement of ceramides in Th17 and iTreg cells
- QUANTIFICATION AND STATISTICAL ANALYSIS
  - Statistical analysis
  - Standardization of gene expression data for metabolic gene identification, T cell-specific GEM reconstruction, and RM analysis
  - Genome-scale metabolic reconstruction and modeling of human CD4$^+$ T cell subsets

REFERENCES

Adam, D., Heinrich, M., Kabelitz, D., and Schütze, S. (2002). Ceramide: Does it matter for T cells? Trends Immunol. *23*, 1–4.

Agren, R., Bordel, S., Mardinoglu, A., Pornputtapong, N., Nookaew, I., and Nielsen, J. (2012). Reconstruction of genome-scale active metabolic networks for 69 human cell types and 16 cancer types using INIT. PLoS Comput. Biol. *8*, e1002518.

Alam, S., Fedier, A., Kohler, R.S., and Jacob, F. (2015). Glucosylceramide synthase inhibitors differentially affect expression of glycosphingolipids. Glycobiology *25*, 351–356.

Apostolidis, S.A., Rauen, T., Hedrich, C.M., Tsokos, G.C., and Crispín, J.C. (2013). Protein phosphatase 2A enables expression of interleukin 17 (IL-17) through chromatin remodeling. J. Biol. Chem. *288*, 26775–26784.

Apostolidis, S.A., Rodríguez-Rodríguez, N., Suárez-Fueyo, A., Dioufa, N., Ozcan, E., Crispín, J.C., Tsokos, M.G., and Tsokos, G.C. (2016). Phosphatase PP2A is requisite for the function of regulatory T cells. Nat. Immunol. *17*, 556–564.

Arvey, A., van der Veeken, J., Samstein, R.M., Feng, Y., Stamatoyannopoulos, J.A., and Rudensky, A.Y. (2014). Inflammation-induced repression of chromatin bound by the transcription factor Foxp3 in regulatory T cells. Nat. Immunol. *15*, 580–587.

Atkinson, M.A., Eisenbarth, G.S., and Michels, A.W. (2014). Type 1 diabetes. Lancet *383*, 69–82. https://doi.org/10.1016/S0140-6736(13)60591-7.

Bai, A., and Guo, Y. (2017). Acid sphingomyelinase mediates human CD4$^+$ T-cell signaling: Potential roles in T-cell responses and diseases. Cell Death Dis. *8*, e2963.

Bai, A., and Robson, S. (2015). Beyond ecto-nucleotidase: CD39 defines human Th17 cells with CD161. Purinergic Signal. *11*, 317–319.

Bai, A., Moss, A., Kokkotou, E., Usheva, A., Sun, X., Cheifetz, A., Zheng, Y., Longhi, M.S., Gao, W., Wu, Y., and Robson, S.C. (2014). CD39 and CD161 modulate Th17 responses in Crohn's disease. J. Immunol. *193*, 3366–3377.

Barbi, J., Pardoll, D., and Pan, F. (2013). Metabolic control of the Treg/Th17 axis. Immunol. Rev. *252*, 52–77.

Berod, L., Friedrich, C., Nandan, A., Freitag, J., Hagemann, S., Harmrolfs, K., Sandouk, A., Hesse, C., Castro, C.N., Bähre, H., et al. (2014). De novo fatty

acid synthesis controls the fate between regulatory T and T helper 17 cells. Nat. Med. 20, 1327–1333.

Bradford, M.M. (1976). A rapid and sensitive method for the quantitation of microgram quantities of protein utilizing the principle of protein-dye binding. Anal. Biochem. 72, 248–254.

Buck, M.D., O'Sullivan, D., and Pearce, E.L. (2015). T cell metabolism drives immunity. J. Exp. Med. 212, 1345–1360.

Cakir, T., Patil, K.R., Onsan, Zi., Ulgen, K.O., Kirdar, B., and Nielsen, J. (2006). Integration of metabolome data with metabolic networks reveals reporter reactions. Mol. Syst. Biol. 2, 50.

Calder, P.C. (1995). Fuel utilization by cells of the immune system. Proc. Nutr. Soc. 54, 65–82.

Carr, E.L., Kelman, A., Wu, G.S., Gopaul, R., Senkevitch, E., Aghvanyan, A., Turay, A.M., and Frauwirth, K.A. (2010). Glutamine uptake and metabolism are coordinately regulated by ERK/MAPK during T lymphocyte activation. J. Immunol. 185, 1037–1044.

Chang, C.-H., and Pearce, E.L. (2016). Emerging concepts of T cell metabolism as a target of immunotherapy. Nat. Immunol. 17, 364.

Chang, C.H., Curtis, J.D., Maggi, L.B., Jr., Faubert, B., Villarino, A.V., O'Sullivan, D., Huang, S.C., van der Windt, G.J., Blagih, J., Qiu, J., et al. (2013). Post-transcriptional control of T cell effector function by aerobic glycolysis. Cell 153, 1239–1251.

Coloff, J.L., Mason, E.F., Altman, B.J., Gerriets, V.A., Liu, T., Nichols, A.N., Zhao, Y., Wofford, J.A., Jacobs, S.R., Ilkayeva, O., et al. (2011). Akt requires glucose metabolism to suppress puma expression and prevent apoptosis of leukemic T cells. J. Biol. Chem. 286, 5921–5933.

Dantzer, R. (2017). Role of the kynurenine metabolism pathway in inflammation-induced depression: Preclinical approaches. Curr. Top. Behav. Neurosci. 31, 117–138.

Dimeloe, S., Burgener, A.V., Grählert, J., and Hess, C. (2017). T-cell metabolism governing activation, proliferation and differentiation; a modular view. Immunology 150, 35–44.

Edgar, R., Domrachev, M., and Lash, A.E. (2002). Gene Expression Omnibus: NCBI gene expression and hybridization array data repository. Nucleic Acids Res. 30, 207–210.

Eisenbarth, G.S. (1986). Type I diabetes mellitus. A chronic autoimmune disease. N. Engl. J. Med. 314, 1360–1368. https://doi.org/10.1056/NEJM198605223142106.

Farrés, M., Platikanov, S., Tsakovski, S., and Tauler, R. (2015). Comparison of the variable importance in projection (VIP) and of the selectivity ratio (SR) methods for variable selection and interpretation. J. Chemometr. 29, 528–536.

Gault, C.R., Obeid, L.M., and Hannun, Y.A. (2010). An overview of sphingolipid metabolism: From synthesis to breakdown. Adv. Exp. Med. Biol. 688, 1–23.

Geiger, R., Rieckmann, J.C., Wolf, T., Basso, C., Feng, Y., Fuhrer, T., Kogadeeva, M., Picotti, P., Meissner, F., Mann, M., et al. (2016). L-Arginine modulates T cell metabolism and enhances survival and anti-tumor activity. Cell 167, 829–842.e13.

Gerriets, V.A., and Rathmell, J.C. (2012). Metabolic pathways in T cell fate and function. Trends Immunol. 33, 168–173.

Hanada, K. (2003). Serine palmitoyltransferase, a key enzyme of sphingolipid metabolism. Biochim. Biophys. Acta 1632, 16–30.

Haug, K., Salek, R.M., Conesa, P., Hastings, J., de Matos, P., Rijnbeek, M., Mahendraker, T., Williams, M., Neumann, S., Rocca-Serra, P., et al. (2013). MetaboLights—An open-access general-purpose repository for metabolomics studies and associated meta-data. Nucleic Acids Res. 41, D781–D786.

Hawkins, R.D., Larjo, A., Tripathi, S.K., Wagner, U., Luu, Y., Lönnberg, T., Raghav, S.K., Lee, L.K., Lund, R., Ren, B., et al. (2013). Global chromatin state analysis reveals lineage-specific enhancers during the initiation of human T helper 1 and T helper 2 cell polarization. Immunity 38, 1271–1284.

Heirendt, L., Arreckx, S., Pfau, T., Mendoza, S.N., Richelle, A., Heinken, A., Haraldsdottir, H.S., Keating, S.M., Vlasov, V., and Wachowiak, J. (2017). Creation and analysis of biochemical constraint-based models: The COBRA toolbox v3.0. arXiv. https://arxiv.org/abs/1710.04038v2.

Hooftman, A., and O'Neill, L.A.J. (2019). The immunomodulatory potential of the metabolite itaconate. Trends Immunol. 40, 687–698.

Hornemann, T., Penno, A., Rütti, M.F., Ernst, D., Kivrak-Pfiffner, F., Rohrer, L., and von Eckardstein, A. (2009). The SPTLC3 subunit of serine palmitoyltransferase generates short chain sphingoid bases. J. Biol. Chem. 284, 26322–26330.

Kallionpää, H., Somani, J., Tuomela, S., Ullah, U., de Albuquerque, R., Lönnberg, T., Komsi, E., Siljander, H., Honkanen, J., Härkönen, T., et al. (2019). Early detection of peripheral blood cell signature in children developing β-cell autoimmunity at a young age. Diabetes 68, 2024–2034.

Kanduri, K., Tripathi, S., Larjo, A., Mannerström, H., Ullah, U., Lund, R., Hawkins, R.D., Ren, B., Lähdesmäki, H., and Lahesmaa, R. (2015). Identification of global regulators of T-helper cell lineage specification. Genome Med. 7, 122.

Kanehisa, M., and Goto, S. (2000). KEGG: Kyoto Encyclopedia of Genes and Genomes. Nucleic Acids Res. 28, 27–30.

Khan, M.M., Ullah, U., Khan, M.H., Kong, L., Moulder, R., Välikangas, T., Bhosale, S.D., Komsi, E., Rasool, O., Chen, Z., et al. (2020). CIP2A constrains Th17 differentiation by modulating STAT3 signaling. iScience 23, 100947.

Klysz, D., Tai, X., Robert, P.A., Craveiro, M., Cretenet, G., Oburoglu, L., Mongellaz, C., Floess, S., Fritz, V., Matias, M.I., et al. (2015). Glutamine-dependent α-ketoglutarate production regulates the balance between T helper 1 cell and regulatory T cell generation. Sci. Signal. 8, ra97.

Lê Cao, K.A., Boitard, S., and Besse, P. (2011). Sparse PLS discriminant analysis: Biologically relevant feature selection and graphical displays for multiclass problems. BMC Bioinformatics 12, 253.

Liblau, R.S., Wong, F.S., Mars, L.T., and Santamaria, P. (2002). Autoreactive CD8 T cells in organ-specific autoimmunity: Emerging targets for therapeutic intervention. Immunity 17, 1–6.

Ma, H., Sorokin, A., Mazein, A., Selkov, A., Selkov, E., Demin, O., and Goryanin, I. (2007). The Edinburgh human metabolic network reconstruction and its functional analysis. Mol. Syst. Biol. 3, 135.

Macintyre, A.N., and Rathmell, J.C. (2013). Activated lymphocytes as a metabolic model for carcinogenesis. Cancer Metab. 1, 5.

MacIver, N.J., Michalek, R.D., and Rathmell, J.C. (2013). Metabolic regulation of T lymphocytes. Annu. Rev. Immunol. 31, 259–283.

Malik-Sheriff, R.S., Glont, M., Nguyen, T.V.N., Tiwari, K., Roberts, M.G., Xavier, A., Vu, M.T., Men, J., Maire, M., Kananathan, S., et al. (2020). BioModels—15 years of sharing computational models in life science. Nucleic Acids Res. 48 (D1), D407–D415.

Mardinoglu, A., Agren, R., Kampf, C., Asplund, A., Uhlen, M., and Nielsen, J. (2014). Genome-scale metabolic modelling of hepatocytes reveals serine deficiency in patients with non-alcoholic fatty liver disease. Nat. Commun. 5, 3083.

Newton, R., Priyadharshini, B., and Turka, L.A. (2016). Immunometabolism of regulatory T cells. Nat. Immunol. 17, 618–625.

Nurieva, R., Wang, J., and Sahoo, A. (2013). T-cell tolerance in cancer. Immunotherapy 5, 513–531.

Nygren, H., Seppänen-Laakso, T., Castillo, S., Hyötyläinen, T., and Orešič, M. (2011). Liquid chromatography-mass spectrometry (LC-MS)-based lipidomics for studies of body fluids and tissues. Methods Mol. Biol. 708, 247–257.

O'Shea, J.J., and Paul, W.E. (2010). Mechanisms underlying lineage commitment and plasticity of helper CD4+ T cells. Science 327, 1098–1102.

O'Sullivan, D., and Pearce, E.L. (2015). Targeting T cell metabolism for therapy. Trends Immunol. 36, 71–80.

Opdam, S., Richelle, A., Kellman, B., Li, S., Zielinski, D.C., and Lewis, N.E. (2017). A systematic evaluation of methods for tailoring genome-scale metabolic models. Cell Syst. 4, 318–329.e6.

Orth, J.D., Thiele, I., and Palsson, B.Ø. (2010). What is flux balance analysis? Nat. Biotechnol. 28, 245–248.

Patil, K.R., and Nielsen, J. (2005). Uncovering transcriptional regulation of metabolism by using metabolic network topology. Proc. Natl. Acad. Sci. USA *102*, 2685–2689.

Pearce, E.L., and Pearce, E.J. (2013). Metabolic pathways in immune cell activation and quiescence. Immunity *38*, 633–643.

Pearce, E.L., Poffenberger, M.C., Chang, C.-H., and Jones, R.G. (2013). Fueling immunity: Insights into metabolism and lymphocyte function. Science *342*, 1242454.

Pedersen, H.K., Forslund, S.K., Gudmundsdottir, V., Petersen, A.Ø., Hildebrand, F., Hyötyläinen, T., Nielsen, T., Hansen, T., Bork, P., Ehrlich, S.D., et al. (2018). A computational framework to integrate high-throughput "-omics" datasets for the identification of potential mechanistic links. Nat. Protoc. *13*, 2781–2800.

Pluskal, T., Castillo, S., Villar-Briones, A., and Oresic, M. (2010). MZmine 2: Modular framework for processing, visualizing, and analyzing mass spectrometry-based molecular profile data. BMC Bioinformatics *11*, 395.

Poffenberger, M.C., and Jones, R.G. (2014). Amino acids fuel T cell-mediated inflammation. Immunity *40*, 635–637.

Powell, J.D., and Delgoffe, G.M. (2010). The mammalian target of rapamycin: Linking T cell differentiation, function, and metabolism. Immunity *33*, 301–311.

Puleston, D.J., Baixauli, F., Sanin, D.E., Edwards-Hicks, J., Villa, M., Kabat, A.M., Kamiński, M.M., Stanckzak, M., Weiss, H.J., Grzes, K.M., et al. (2021). Polyamine metabolism is a central determinant of helper T cell lineage fidelity. Cell *184*, 4186–4202.e20.

Ritchie, M.E., Phipson, B., Wu, D., Hu, Y., Law, C.W., Shi, W., and Smyth, G.K. (2015). limma powers differential expression analyses for RNA-sequencing and microarray studies. Nucleic Acids Res. *43*, e47.

Ryan, D.G., and O'Neill, L.A.J. (2017). Krebs cycle rewired for macrophage and dendritic cell effector functions. FEBS Lett. *591*, 2992–3006.

Sattar, N., McInnes, I.B., and McMurray, J.J.V. (2020). Obesity is a risk factor for severe COVID-19 infection: Multiple potential mechanisms. Circulation *142*, 4–6.

Sen, P., Kemppainen, E., and Orešič, M. (2018). Perspectives on systems modeling of human peripheral blood mononuclear cells. Front. Mol. Biosci. *4*, 96.

Sen, P., Dickens, A.M., López-Bascón, M.A., Lindeman, T., Kemppainen, E., Lamichhane, S., Rönkkö, T., Ilonen, J., Toppari, J., Veijola, R., et al. (2020). Metabolic alterations in immune cells associate with progression to type 1 diabetes. Diabetologia *63*, 1017–1031.

Sugiura, A., and Rathmell, J.C. (2018). Metabolic barriers to T cell function in tumors. J. Immunol. *200*, 400–407.

Thiele, I., and Palsson, B.O. (2010). A protocol for generating a high-quality genome-scale metabolic reconstruction. Nat. Protoc. *5*, 93–121.

Thiele, I., Swainston, N., Fleming, R.M., Hoppe, A., Sahoo, S., Aurich, M.K., Haraldsdottir, H., Mo, M.L., Rolfsson, O., Stobbe, M.D., et al. (2013). A community-driven global reconstruction of human metabolism. Nat. Biotechnol. *31*, 419–425.

Tripathi, S.K., Chen, Z., Larjo, A., Kanduri, K., Nousiainen, K., Äijo, T., Ricaño-Ponce, I., Hrdlickova, B., Tuomela, S., Laajala, E., et al. (2017). Genome-wide analysis of STAT3-mediated transcription during early human Th17 cell differentiation. Cell Rep. *19*, 1888–1901.

Trupp, M., Altman, T., Fulcher, C.A., Caspi, R., Krummenacker, M., Paley, S., and Karp, P.D. (2010). Beyond the genome (BTG) is a (PGDB) pathway genome database: HumanCyc. Genome Biol. *11* (*Suppl 1*), O12.

Tuomela, S., and Lahesmaa, R. (2013). Early T helper cell programming of gene expression in human. Semin. Immunol. *25*, 282–290.

Tuomela, S., Rautio, S., Ahlfors, H., Öling, V., Salo, V., Ullah, U., Chen, Z., Hämälistö, S., Tripathi, S.K., Äijö, T., et al. (2016). Comparative analysis of human and mouse transcriptomes of Th17 cell priming. Oncotarget *7*, 13416–13428.

Ubaid Ullah, Andrabi, S.B.A., Tripathi, S.K., Dirasantha, O., Kanduri, K., Rautio, S., Gross, C.C., Lehtimäki, S., Bala, K., Tuomisto, J., et al. (2018). Transcriptional repressor HIC1 contributes to suppressive function of human induced regulatory T cells. Cell Rep. *22*, 2094–2106.

Virtue, S., and Vidal-Puig, A. (2010). Adipose tissue expandability, lipotoxicity and the metabolic syndrome—An allostatic perspective. Biochim. Biophys. Acta *1801*, 338–349.

Wagner, A., Wang, C., Fessler, J., DeTomaso, D., Avila-Pacheco, J., Kaminski, J., Zaghouani, S., Christian, E., Thakore, P., Schellhaass, B., et al. (2021). Metabolic modeling of single Th17 cells reveals regulators of autoimmunity. Cell *184*, 4168–4185.e21.

Wang, H., Marcišauskas, S., Sánchez, B.J., Domenzain, I., Hermansson, D., Agren, R., Nielsen, J., and Kerkhoven, E.J. (2018). RAVEN 2.0: A versatile toolbox for metabolic network reconstruction and a case study on *Streptomyces coelicolor*. PLoS Comput. Biol. *14*, e1006541.

Wang, F., Hou, H., Luo, Y., Tang, G., Wu, S., Huang, M., Liu, W., Zhu, Y., Lin, Q., Mao, L., et al. (2020). The laboratory tests and host immunity of COVID-19 patients with different severity of illness. JCI Insight *5*, e137799.

Westerhuis, J.A., Hoefsloot, H.C., Smit, S., Vis, D.J., Smilde, A.K., van Velzen, E.J., van Duijnhoven, J.P., and van Dorsten, F.A. (2008). Assessment of PLSDA cross validation. Metabolomics *4*, 81–89.

Wu, D., and Yang, X.O. (2020). TH17 responses in cytokine storm of COVID-19: An emerging target of JAK2 inhibitor fedratinib. J. Microbiol. Immunol. Infect. *53*, 368–370.

Xu, Q., Jin, X., Zheng, M., Rohila, D., Fu, G., Wen, Z., Lou, J., Wu, S., Sloan, R., Wang, L., et al. (2019). Phosphatase PP2A is essential for T_H17 differentiation. Proc. Natl. Acad. Sci. USA *116*, 982–987.

Zhang, T., de Waard, A.A., Wuhrer, M., and Spaapen, R.M. (2019). The role of glycosphingolipids in immune cell functions. Front. Immunol. *10*, 90.

Zhu, J., and Paul, W.E. (2008). CD4 T cells: Fates, functions, and faults. Blood *112*, 1557–1569.

Zur, H., Ruppin, E., and Shlomi, T. (2010). iMAT: An integrative metabolic analysis tool. Bioinformatics *26*, 3140–3142.

STAR★METHODS

KEY RESOURCES TABLE

REAGENT or RESOURCE	SOURCE	IDENTIFIER
Chemicals, peptides, and recombinant proteins		
2-diheptadecanoyl-sn-glycero-3-phosphoethanolamine (PE(17:0/17:0))	Avanti Polar Lipids	Cat#830756
N-heptadecanoyl-D-erythro-sphingosylphosphorylcholine (SM(d18:1/17:0))	Avanti Polar Lipids	Cat#860585
1-stearoyl-2-hydroxy-sn-glycero-3-phosphocholine (LPC(18:0))	Avanti Polar Lipids	Cat#855775
2-diheptadecanoyl-sn-glycero-3-phosphocholine (PC(17:0/17:0))	Avanti Polar Lipids	Cat#850360
1-heptadecanoyl-2-hydroxy-sn-glycero-3-phosphocholine (LPC(17:0))	Avanti Polar Lipids	Cat#855676
2-Dioctadecanoyl- -sn-glycero-3-phosphocholine (PC(18:0/18:0))	Avanti Polar Lipids	Cat#850333
1-Hexadecanoyl-2-oleoyl-sn-glycero-3-phosphocholine (PC(16:0/18:1)	Avanti Polar Lipids	Cat#850457
1-(9Z-octadecenoyl)-sn-glycero-3-phosphoethanolamine (LPE(18:1))	Avanti Polar Lipids	Cat#850456
1-Palmitoyl-2-Hydroxy-sn-Glycero-3-Phosphatidylcholine (LPC(16:0))	Avanti Polar Lipids	Cat#846725
triheptadecanoylglycerol (TG(17:0/17:0/17:0))	Larodan	Cat#33-1700
trihexadecanoalglycerol (TG(16:0/16:0/16:0))	Larodan	Cat#33-1610
1-stearoyl-2-linoleoyl-sn-glycerol (DG(18:0/18:2))	Avanti Polar Lipids	Cat#855675
3-trioctadecanoylglycerol (TG(18:0/18:0/18:0))	Larodan	Cat#33-1810
3β-Hydroxy-5-cholestene-3-linoleate (ChoE(18:2))	Larodan	Cat#64-1802
1-hexadecyl-2-(9Z-octadecenoyl)-sn-glycero-3-phosphocholine (PC(16:0e/18:1(9Z)))	Avanti Polar Lipids	Cat#800817
1-(1Z-octadecanyl)-2-(9Z-octadecenoyl)- sn-glycero-3-phosphocholine (PC(18:0p/18:1(9Z)))	Avanti Polar Lipids	Cat#878112
1-oleoyl-2-hydroxy-sn-glycero-3-phosphocholine (LPC(18:1))	Larodan	Cat#38-1801
1-palmitoyl-2-oleoyl-sn-glycero-3-phosphoethanolamine (PE(16:0/18:1))	Avanti Polar Lipids	Cat#852467
3β-hydroxy-5-cholestene-3-stearate (ChoE(18:0))	Larodan	Cat#64-1800
1-palmitoyl-d31-2-oleoyl-sn-glycero-3-phosphocholine (PC(16:0/d31/18:1))	Avanti Polar Lipids	Cat#850757
Lactosyl(β) ceramide (D18:1/17:0)	Avanti Polar Lipids	Cat#878130
C17 Glucosyl(β) ceramide (D18:1/17:0)	Avanti Polar Lipids	Cat#860399
C17 ceramide (D18:1/17:0)	Avanti Polar Lipids	Cat#860595
Deuterated Ceramide LIPIDOMIX® Mass Spec Standard	Avanti Polar Lipids	Cat#860569
Glucosyl (β) C12 ceramide	Avanti Polar Lipids	Cat#860517
Lactosyl (β) C12 ceramide	Avanti Polar Lipids	Cat#330713
C18 ceramide (D18:1/18:1)	Avanti Polar Lipids	Cat#860543
C18:1 dihydroceramide (d18:0/18:1(9Z))	Avanti Polar Lipids	Cat#860545
Experimental models		
Human CD4^{+} T cells		

(Continued on next page)

Continued

REAGENT or RESOURCE	SOURCE	IDENTIFIER
Deposited data		
Lipidomics raw and analyzed data deposited (this paper)	Metabolomics Workbench	Project ID PR001078. (https://doi.org/10.21228/M8C111)
Gene expression and transcriptomics data retrieved for human CD4+ T cells subsets and their paired controls (Th0).	NCBI Gene Expression Omnibus (GEO) repository	Thp, Th1 and Th2 (Kanduri et al., 2015), Th17 (Tuomela et al., 2016) and iTreg cells (Ubaid Ullah et al., 2018) Accession numbers: GSE71646, GSE52260 and GSE90570 respectively.
Transcriptomic (RNASeq) datasets for CD4+ and PBMCs isolated from children at risk of Type 1 Diabetes (T1D) (Kallionpää et al., 2019)	European genome-phenome archive	Accession number: EGAC00001001443
Genome-scale metabolic models for CD4+ T cell subsets (this paper)	BioModels	ID: MODEL2101270002
Software and algorithms		
R v3.6.0	Hosted by Vienna, University of Economics	https://cran.r-project.org/
MATLAB 2017b	Mathworks, Inc., (Natick, MA, USA)	https://se.mathworks.com/
Cobra toolbox v3.0	Heirendt et al., 2017	https://opencobra.github.io/
RAVEN 2.0 suite	Wang et al., 2018	https://github.com/SysBioChalmers/RAVEN
ImageJ	Developed at the National Institute of Health and the Laboratory for Optical and Computational Instrumentation	https://imagej.nih.gov/ij/docs/menus/analyze.html

RESOURCE AVAILABILITY

Lead contact

Further information and requests for resources and reagents should be directed to and will be fulfilled by the Lead Contact, Matej Orešič (matej.oresic@oru.se).

Materials availability

This study did not generate new unique reagents.

Data and code availability

- The lipidomic datasets generated in this study is available at the NIH Common Fund's National Metabolomics Data Repository (NMDR) website, the Metabolomics Workbench (https://www.metabolomicsworkbench.org), where it has been assigned a Project ID: *PR001078*. The data can be accessed directly via it's Project DOI: 10.21228/M8C111. The GEMs for human CD4+ T cell subsets were deposited in BioModels (Malik-Sheriff et al., 2020) (https://www.ebi.ac.uk/biomodels/), and assigned an identifier: *MODEL2101270002.*
- This paper does not report original code.
- Any additional information required to reanalyze the data reported in this work paper is available from the Lead Contact upon request.

EXPERIMENTAL MODEL AND SUBJECT DETAILS

Human experiments

Human CD4+ T cells isolated from the human umbilical cord blood as described previously (Hawkins et al., 2013; Khan et al., 2020; Tripathi et al., 2017; Ubaid Ullah et al., 2018). The use of the blood of unknown donors was approved by the Ethics Committee of the Hospital District of Southwest Finland (24.11.1998, article 323).

METHOD DETAILS

Human CD4$^+$ T cell isolation, activation, and differentiation

CD4$^+$ T cells were isolated from umbilical cord blood as described previously by (Hawkins et al., 2013; Khan et al., 2020; Tripathi et al., 2017; Ubaid Ullah et al., 2018). Human umbilical cord blood was layered on ficol (GE Healthcare, cat# 17-1440-03) for isolation of white blood cells. CD4$^+$ T cells were then isolated using the bead-based CD4$^+$ isolation kit from Invitrogen (cat# 11331D). For activation of T cells, a combination of plate-bound anti-CD3 (3750 ng/6-well culture plate well) (Beckman Coulter, cat# IM-1304) and soluble anti-CD28 (1 μg/mL)(Beckman Coulter, cat# IM1376) antibodies were used.

For Th17 cell differentiation, isolated CD4$^+$ cells were activated with a combination of plate-bound anti-CD3 (750 ng/24-well culture plate well; Immunotech/Beckman Coulter REF # IM-1304) and soluble anti-CD28 ((1ug/mL; Immunotech/Beckman coulter REF # IM1376) antibodies in serum-free X-Vivo 20 medium (Lonza), in the absence (Th0) or presence (Th17) of IL-6 (20ng/ml, Roche, Cat# 11138600 001); IL-1β (10ng/ml, R&D Systems Cat # 201 LB); TGF-β1 (10ng/ml, R&D Systems Cat# 240); anti-IL-4 (1 μg/ml) R&D Systems Cat# MAB204) and anti-IFN-γ (1 μg/ml R&D Systems Cat#MAB-285). Differentiation of Th17 cells was confirmed by measuring IL-17 expression by quantitative real-time PCR, at 72 hours of Th17/Th0 culturing (Khan et al., 2020).

For iTreg cell culturing, after CD25$^+$ cells were depleted using LD columns from CD25 depletion kit (Miltenyi Biotec), CD4$^+$CD25$^-$ cells were activated with plate-bound anti-CD3 (500 ng/24-well culture plate well) and soluble anti-CD28 (500 ng/mL) at a density of 2 × 10^6 cells/mL of X-vivo 15 serum-free medium (Lonza). For iTreg differentiation, the medium was supplemented with IL-2 (12 ng/mL), TGF-β (10 ng/mL) (both from R&D Systems), all-trans retinoic acid (ATRA) (10 nM; Sigma-Aldrich), and human serum (10%) and cultured at 37°C in 5% CO$_2$. Control Th0 cells were stimulated with plate-bound anti-CD3 soluble anti-CD28 antibodies without cytokines. For confirmation of iTreg cell differentiation, we used intracellular staining to measure, at 72 hours of iTreg culturing, expression of FOXP3 which is the major transcription factor driving Treg differentiation. Intracellular staining was performed using buffer sets of Human Regulatory T cell Staining Kit (eBioscience/Thermo Fisher Scientific), following the manufacturer's protocol. The following antibodies were used: anti-human FOXP3-PE (eBioscience, Cat. No. 12-4776-42) and rat IgG2a isotype control (eBioscience, Cat. No. 72-4321-77A). All samples were acquired by a flow cytometer (LSRII) and analyzed either with FlowJo (FLOWJO, LLC) or with Flowing Software (Ubaid Ullah et al., 2018).

Th1 and Th2 cell differentiation were done as described previously (Hawkins et al., 2013). Briefly, purified naive CD4$^+$ T cells were activated with plate-bound anti-CD3 (500 ng/24-well culture plate well) and 500 ng/ml soluble anti-CD28 and cultured in the absence (Th0) or presence of 2.5 ng/ml IL-12 (R&D Systems) (Th1) or 10 ng/ml IL-4 (R&D Systems) (for Th2). At 48 hours following the activation of the cells, 17 ng/ml IL-2 (R&D Systems) was added to the cultures. Differentiation of Th1 and Th2 cells was confirmed by measuring (using flow cytometry) the expression of T-bet and Gata3 at 72 hours after cell activation. Briefly, cells were fixed and permeabilized using the Intracellular Fixation & Permeabilization Buffer Set (eBioscience/Thermo Fisher Scientific), according the manufacturer's protocol. The following antibodies were used: anti-human GATA3-PE (eBioscience, 12-9966), anti-human T-bet-BV711 (BD, 563320) and corresponding isotype controls (BV711 Mouse IgG1, BD, 563044 and PE Rat IgG2b, eBioscience, 12-4031-82). Samples were acquired by BD LSRFortessa cell analyzer and data were analyzed using FlowJo software (FLOWJO, LLC).

siRNA-mediated gene knockdown

For *SPTLC* triple knock down (TKD) and *UGCG* single knock down (KD) experiments, freshly-isolated CD4$^+$ cells were suspended in Optimem I (Invitrogen) and transfected with siGenome SMARTpool small interference RNA (siRNA) oligonucleotides (Dharmacon) using the nucleofection technique by Lonza. Scrambled non-targeting siRNA (5′-AAUUCUCCGAACGUGUCACGU-3′) was used as control (Sigma). Briefly, four million cells were transfected with 12 μg of *SPTLC*-targeting siRNAs (4 μg of SMARTpool *SPTLC1* siRNA M-006673-02; 4 μg of SMARTpool *SPTLC2* siRNA M-006674-01; and 4 μg of SMARTpool *SPTLC3* siRNA M-010285-02) or 12 μg of Scramble siRNA. For UGCG single knockdown experiments 12 μg of UGCG-targeting siRNA (siGenome SMARTpool, M-006441-02) were used. Cells were rested for 24h in RPMI 1640 medium (Sigma-Aldrich) supplemented with penicillin/streptomycin, 2 mM L-glutamine and 10% FCS and subsequently activated and cultured under Th17 conditions. *SPTLC1* and *SPTLC2* knockdown was validated by western blot at 24 hours, *UGCG* and *SPTLC3* knockdown was determined using quantitative real-time PCR (at 12 and 72 hours, respectively).

Western blot

Fresh cell samples were lysed in RIPA buffer (Thermo) supplemented with complete EDTA-free Protease inhibitor cocktail and phosphatase inhibitors (Roche) and sonicated on a Bioruptor (Diagenode). Protein concentration was determined using DC Protein assay (Biorad). After boiling in 6 × loading dye (330 mM Tris-HCl, pH 6.8; 330 mM SDS; 6% β-ME; 170 μM bromophenol blue; 30% glycerol), the samples were loaded on Mini-PROTEAN TGXPrecast Protein Gels (BioRad Laboratories) and transferred to PVDF membranes (Trans-Blot TurboTransfer Packs, BioRad Laboratories). The following primary antibodies were used: *SPTLC1* (sc-374143, Santa Cruz), *SPTLC2* (ab236900, abcam) and beta-actin (A5441, Sigma-Aldrich).

Quantitative real-time PCR

Total RNA was extracted using the AllPrep DNA/RNA/miRNA Universal Kit (QIAGEN) and treated in-column with DNase (RNase-Free Dnase Set; QIAGEN) for 15 minutes. For quantitative real-time PCR purified RNA was treated with DNase I (Invitrogen) to ensure

complete removal of genomic DNA followed by cDNA synthesis with SuperScript II Reverse Transcriptase (Invitrogen). Quantitative real-time PCR (qPCR) was performed using the TaqMan® Gene Expression *UGCG* Assay ID:Hs00916612_m1 and SPTLC3 Assay ID:Hs00217867_m1 (Thermo Fisher Scientific) or KAPA probe fast qPCR Master Mix (Kapa Biosystems) and Universal ProbeLibrary probes (Roche Applied Science) with custom ordered primers. The qPCR runs were analyzed with Applied Biosystems QuantStudio 12K Flex Real-Time PCR System. All reactions were performed in triplicate.

Analysis of molecular lipids

The samples were randomized and extracted using a modified version of the previously-published Folch procedure (Pedersen et al., 2018). Briefly, 150 μL of 0.9% NaCl was added to cell pellets, and samples then vortexed and ultrasonicated for 3 minutes. Next, 20 μL of the cell suspension was mixed with 150 μL of the 2.5 μg mL^{-1} internal standards solution in ice-cold CHCl3:MeOH (2:1, v/v). The internal standard solution contained the following compounds: 1,2-diheptadecanoyl-sn-glycero-3-phosphoethanolamine (PE (17:0/17:0)), N-heptadecanoyl-D-erythro-sphingosylphosphorylcholine (SM(d18:1/17:0)), N-heptadecanoyl-D-erythro-sphingosine (Cer(d18:1/17:0)), 1,2-diheptadeca-noyl-sn-glycero-3-phosphocholine (PC(17:0/17:0)), 1-heptadecanoyl-2-hydroxy-sn-glycero-3-phosphocholine (LPC(17:0)) and 1-palmitoyl-d31-2-oleoyl-sn-glycero-3-phosphocholine (PC(16:0/d31/18:1)). These were purchased from Avanti Polar Lipids, Inc. (Alabaster, AL, USA). In addition, triheptadecanoin (TG(17:0/17:0/17:0)) was purchased from (Larodan AB, (Solna, Sweden). The samples were vortexed and incubated on ice for 30 min after which they were centrifuged at 7800 × g for 5 min. Finally, 60 μL from the lower layer of each sample was collected and mixed with 60 μL of ice cold CHCl3:MeOH (2:1, *v/v*) in LC vial. The total protein content in cells was measured by the Bradford method(Bradford, 1976).

The UHPLC-QTOFMS analyses were done in a similar manner to as described earlier, with some modifications (Nygren et al., 2011; Pedersen et al., 2018) on two separate instruments. The initial lipidomic results were acquired on a UHPLC-QTOFMS system from Agilent Technologies (Santa Clara, CA, USA) combining a 1290 Infinity LC system and 6545 quadrupole time of flight mass spectrometer (QTOFMS), interfaced with a dual jet stream electrospray (dual ESI) ion source. MassHunter B.06.01 software (Agilent Technologies, Santa Clara, CA, USA) was used for all data acquisition. The SM results for *UGCG*-silenced Th17 cells data were acquired on a UHPLC-QTOF system from Bruker (Bruker, Billerica, MA, USA) combining an Elute UHPLC binary pump and an Impact II system QTOF system. The samples for this experiments were the same extracts that the Cer data were acquired from and had SM(18:1/17:0) spiked in prior to acquisition. The data were acquired using the Hystar suite of software. MZmine 2 was used for all the untargeted data processing (Pluskal et al., 2010).

Chromatographic separation was performed using an Acquity UPLC BEH C18 column (100 mm × 2.1 mm i.e., 1.7 μm particle size) and protected using a C18 precolumn, both from Waters Corporation (Wexford, Ireland). The mobile phases were water (phase A) and acetonitrile:2-propanol (1:1, *v/v*) (phase B), both containing 1% 1M ammonium acetate and 0.1% (*v/v*) formic acid ammonium acetate as ionization agents. The LC pump was programmed at a flow rate of 0.4 mL min^{-1} and the elution gradient was as follows: from min 0–2, the percentage of phase B was modified from 35% to 80%, from min 2-7, the percentage of phase B was modified from 80% to 100% and this final percentage held for 7 min. A post-time of 7 min was used to regain the initial conditions for the next analysis. Thus, the total analysis time per sample was 21 min (including postprocessing). The settings of the dual ESI ionization source were as follows: capillary voltage 3.6 kV, nozzle voltage 1500 V, N_2 pressure in the nebulizer 21 psi, N_2 flow rate and temperature as heat gas 11 L min^{-1} and 379°C, respectively. Accurate mass spectra in MS scan were acquired in the m/z range 100 – 1700 in positive ion mode.

MS data were processed using the open source software MZmine 2.53 (Pluskal et al., 2010). The following data processing steps were applied to the raw MS data: (1) Crop filtering with a m/z range of 350 – 1200 m/z and a retention time (RT) range of 2 to 15 minutes; (2) Mass detection with a noise level of 900; (3) Chromatogram builder with a min time span of 0.08 minutes, minimum height of 900 and m/z tolerance of 0.006 m/z or 10.0 ppm; (4) Chromatogram deconvolution using the local minimum search algorithm with a 70% chromatographic threshold, 0.05 min minimum RT range, 5% minimum relative height, 1200 minimum absolute height, a minimum ration of peak top/edge of 1.2 and a peak duration range of 0.08 - 1.01 minutes; (5) Isotopic peak grouper with a m/z tolerance of 5.0 ppm, RT tolerance of 0.05 minute, maximum charge of 2 and with the most intense isotope set as the representative isotope; (6) Join aligner with m/z tolerance of 0.009 or 10.0 ppm and a weight of 2, RT tolerance of 0.1 minute and a weight of 1 and with no requirement of charge state or ID and no comparison of isotope pattern; (7) Peak list row filter with a minimum of 7 peaks in a row (10% of the samples); (8) Gap filling using the same RT and m/z range gap filler algorithm with an m/z tolerance of 0.009 m/z or 11.0 ppm; (9) Identification of lipids using a custom database (based on UHPLC-MS/MS data using the same lipidomics protocol, with RT data and MS and MS/MS) search with an m/z tolerance of 0.009 m/z or 10.0 ppm and a RT tolerance of 0.2 min. In general, lipids were identified at the total number of carbons and double bonds in the structure as there was insufficient evidence to assign the specific acyl chains. Where the acyl chains are identified these have been confirmed with MS/MS level experiments and/or authentic standards. (10) Normalization using internal standards (PE (17:0/17:0), SM (d18:1/17:0), Cer (d18:1/17:0), LPC (17:0), TG (17:0/17:0/17:0) and PC (16:0/d30/18:1)) for identified lipids and closest internal standard (based on RT) for the unknown lipids, followed by calculation of the concentrations based on lipid-class calibration curves.

Identification of lipids was done using an in-house spectral library with MS (and retention time), MS/MS information, and by searching the LIPID MAPS spectral database (https://www.lipidmaps.org/). MS/MS data were acquired in both negative and positive ion modes in order to maximize identification coverage. Additionally, some lipids were verified by injection of commercial standards. The identification was carried out in pooled cell extracts.

The peak area obtained for each lipid was normalized with lipid-class specific internal standards and with total content of protein. A (semi) quantitation was performed using lipid-class specific calibration curves. Pooled cell extracts were used for quality control, in addition to in-house plasma. The raw variation of the peak areas of internal standards in the samples was on average 15.3% and the RSD of retention times of identified lipids across all samples was on average 0.28%. The RSD of the concentrations of the identified lipids in QC samples and pooled extracts was on average 17.7%.

Measurement of ceramides in Th17 and iTreg cells
Sample extraction
The frozen cell preps were defrosted on ice. The samples were extracted using a modified Folch method (Sen et al., 2020). Briefly, 120 μL of cold (4°C) extraction solvent (CHCl$_3$: MeOH, (2:1 v/v) was added to the samples. The extraction solvent containing the following internal standards: C17 Lactosyl(β) ceramide (D18:1/17:0, 20 ppb), C17 Glucosyl(β) ceramide (D18:1/17:0, 20 ppb), C17 ceramide (D18:1/17:0, 20 ppb), C16 ceramide-d7 (d18:1-d7/16:0, 16,57 ppb), C18 ceramide-d7 (d18:1-d7/18:0, 8.75 ppb), C24 ceramide-d7 (d18:1-d7/24:0, 20 ppb), and C24:1 ceramide-d7 (d18:1-d7/24:1(15Z), 9,96 ppb). The samples were the vortexed briefly and left on ice for 30 minutes. The samples were then centrifuged (9400 g, 5 min, 4°C) and then 60 μL of the bottom layer was transfer to a clean mass spectrometry vial (2 mL). The samples were then stored at –80°C.

Mass spectrometry
The ceramides were quantified using a targeted multiple reaction monitoring (MRM) method using UHPLC as a separation technique. The LC separation was based on the global lipidomics method previously described(Sen et al., 2019). Briefly, the UHPLC was a Exion AD (Sciex) integrated system. The samples were held in a cool box at 15°C prior to the analysis. The needle was washed with both a 10% DCM in MeOH and ACN: MeOH: IPA: H$_2$O (1:1:1:1 v/v/v/v) with 1% HCOOH for a total of 7.5 s each. The solvents were delivered using a quaternary solvent and a column oven (set to 50°C). The separation was performed on an ACQUITY UHPLC BEH C18 column (2.1 mm × 100 mm, particle size 1.7 μm, Waters, Milford, MA, USA). The flow rate was set at 0.4 ml/min throughout the run with an injection volume of 1 μL. The following solvents were used for the gradient elution: Solvent A was H$_2$O with 1% NH$_4$Ac (1M) and HCOOH (0.1%) added. Solvent B was a mixture of ACN: IPA (1:1 v/v) with 1% NH$_4$Ac (1M) and HCOOH (0.1%) added. The gradient was programmed as follows: 0 to 2 min 35%–80% B, 2 to 7 min 80%–100% B, 7 to 14 min 100% B. The column was equilibrated with a 7min period of 35% B prior to the next run. The mass spectrometer was a Sciex 5500 QTRAP (Sciex) set in scheduled MRM mode. The details of the MRM transitions can be seen in (Table S1). All lipids were identified for their fatty acid composition by MS/MS to confirm their exact identification, there was also a linear relationship between the increasing number of carbons in the lipid chain and its corresponding retention time. Due to the isobaric nature of sugars we were unable to differentiate Glc and Glc head groups. All data were integrated using the quantitation tool in MultiQuant (3.0.3), all peaks were manually checked. Any analytes which were over the concentration of the standard curve were diluted (1:25) with the same extraction solvent minus the internal standards. The quantification was performed using class-based internal standards and in the case of those ceramide species without an authentic standard in the standard curve mix, we used the closest related structure. The standard curve mixture contained: Glucosyl (β) C12 ceramide, Lactosyl (β) C12 ceramide, C18 ceramide (D18:1/18:1), C18:1 dihydroceramide (d18:0/18:1(9Z)) and was run at the following levels (all in ppb): 100, 80, 60, 50, 40, 30, 20, 10 for the C12 standards and 10, 8, 6, 5, 4, 3, 2,1 for all C18 standards.

QUANTIFICATION AND STATISTICAL ANALYSIS

Statistical analysis
The lipidomic dataset was log$_2$ transformed. Principal component analysis (PCA) was performed using 'prcomp' function included in the 'stats' R package, no outliers found. Sparse Partial Least-squares Discriminant Analysis (sPLS-DA) (Lê Cao et al., 2011) of the T cell subsets was performed using the 'splsda' function coded in the 'mixOmics v6.3.2' R package. In addition, several PLS-DA models between Th0 versus Thp, Th1 versus Th0, Th2 versus Th0, Th17 versus Th0 and iTreg versus Th0 cells were developed and Variable Importance in Projection (VIP) scores (Farrés et al., 2015) were estimated. The PLS-DA models were cross-validated (Westerhuis et al., 2008) by 7-fold cross-validation and model diagnostics were generated using 'perf' function.

The multivariate PLS-DA analysis was followed by a univariate statistic; a paired t test using the 't.test' function was performed to identify significant differences in the lipid intensities between T cell subsets and their paired control (Th0). All lipids that passed one or more criteria for variable selection, i.e., with the sPLS-DA model with an area under the ROC curve (AUC) > = 0.85; RC (> ± 0.05), VIP scores > 1 or paired t test; p.adj < 0.05) were listed as significant. All the initial / nominal p values were subjected to multiple hypothesis testing correction, vis-à-vis False Discovery Rate (FDR) adjustment using the 'p-adjust' function. The 'Heatmap.2', 'boxplot', 'beanplot', 'gplot', and 'ggplot2' libraries/packages were used for data visualization.

Standardization of gene expression data for metabolic gene identification, T cell-specific GEM reconstruction, and RM analysis
Lineage-specific normalized gene expression profiles of the human CD4$^+$ Thp, Th1 and Th2 (Kanduri et al., 2015), Th17 (Tuomela et al., 2016), iTreg cells (Ubaid Ullah et al., 2018) and their paired control (Th0) were obtained from the literature and/or Gene Expression Omnibus (GEO) (https://www.ncbi.nlm.nih.gov/geo/) (Edgar et al., 2002) with the accession numbers (Thp, Th1 & Th2, *GEO: GSE71646*), (Th17, *GEO: GSE52260*) and (iTreg, *GEO: GSE90570*) respectively. Differentially-expressed genes for each T cell subset

versus Th0 were estimated using *limma* R/Bioconductor package/pipeline (Ritchie et al., 2015) with eBayes and 'treat' methods. Genes that were differentially-expressed (p < 0.05, adjusted for FDR) between a pair of condition were listed.

These expression datasets of the human CD4+ T cells (Thp, Th1 and Th2 (Kanduri et al., 2015), Th17 (Tuomela et al., 2016), iTreg cells (Ubaid Ullah et al., 2018), and their paired control (Th0)) were used for the identification of MGs. Furthermore, they were used for the contextualization of HTimmR to T cell-specific GEMs.

In order to identify MGs, genes expressed in Thp, Th1, Th2, Th17 and iTreg cells were searched in the existing human metabolic reconstructions, i.e., HMR2 (Mardinoglu et al., 2014), Edinburgh Human Metabolic Network (ETHMN) (Ma et al., 2007), RECON2 (Thiele et al., 2013), and databases, i.e., the Kyoto Encyclopedia of Genes and Genomes (KEGG) (Kanehisa and Goto, 2000) and the Encyclopedia of Human Genes and Metabolism (HumanCyc) (Trupp et al., 2010). We found that HMR2 had the highest coverage of the MGs from our datasets. However, 160 MGs were missing in HMR2 and other metabolic reconstructions. Metabolic reactions (MRs) encoded by these genes were identified from the literature. These MRs were used for the reconstruction of HTimmR (Data S1).

Genome-scale metabolic reconstruction and modeling of human CD4+ T cell subsets
Contextualization of HTimmR to CD4+ T helper-specific GEMs
Functional GEMs of Thp, Th1, Th2, Th17 and iTreg cells were developed by INIT (Agren et al., 2012) algorithm applied to HTimmR, used as a template model. HTimmR model was contextualized for each CD4+ T cell subset using lineage-specific gene expression data for human CD4+ Thp, Th1 and Th2 (Kanduri et al., 2015), Th17 (Tuomela et al., 2016), iTreg cells (Ubaid Ullah et al., 2018), and their paired control (Th0). The subset-specific expression data were used to score the reactions in the HTimmR model in order to evaluate the likelihood of a metabolic reaction being present or absent in a T cell subset model. Threshold for high and low expressed genes was determined by (mean ± sd) of log-normal distribution of the expression data (Opdam et al., 2017; Zur et al., 2010). The expression data were mapped to HTimmR using gene-protein-reaction association (GPR) rules, and reaction scores were generated. The mapping was performed using *'mapExpressionToReactions'* function coded in COBRA toolbox (Heirendt et al., 2017). The reaction scores were used as input to the INIT algorithm (Agren et al., 2012).

Subsequently, draft GEMs for CD4+ T cell subsets that includes the active metabolic reactions and their associated components (e.g., metabolic genes, enzymes, metabolites, and their interactions) was generated. A quality control/sanity check (Thiele and Palsson, 2010) was performed using COnstraint-Based Reconstruction and Analysis Toolbox (COBRA toolbox v3.0) (Heirendt et al., 2017). Any blocked reactions were rectified or removed before knockout and flux analysis was performed. Mixed integer linear programming (MILP) was performed using *'MOSEK 8'* solver (licensed for the academic user) integrated in the RAVEN 2.0 suite (Wang et al., 2018). Linear programming (LP) and optimization was performed using *'ILOG-IBM CPLEX (version 128)'* solver.

A similar approach was taken to develop and contextualize cell-specific GEMs for CD4+ T cells and PBMCs from children at risk of T1D using transcriptomic (RNASeq) datasets (European genome-phenome archive (Kallionpää et al., 2019) accession number: *EGAC00001001443*) of these immune cell subsets and PBMCs. The metabolomics data of the PBMCs were retrieved from the MetaboLights (Haug et al., 2013) (accession number: *MTBLS1015*).

Reporter metabolite analysis
The lineage-specific, differentially-expressed MGs identified in this study from different human CD4+ T cell subsets was employed for the RM predictions. RM analysis was performed using the *'reporterMetabolites'* function of the RAVEN 2.0 suite (Wang et al., 2018).

Overrepresentation analysis (ORA) of the RMs in the metabolic subsystems/pathways of human CD4+ T cell subset was evaluated by a global hypergeometric test. RMs that were significantly (p < 0.05, adjusted for FDR) altered between the T cell subsets versus Th0 were subjected to ORA. All the metabolic subsystems/pathways with (q-values = p < 0.05, adjusted for FDR) were listed.

Reaction knockout and essentiality analysis
An *in-silico* knockout (KO) analysis of the reactions of sphingolipid pathway toward Cer biosynthesis in CD4+ Th17 cells was performed. Here, we evaluated the ability of a metabolic reaction to produce Cers in a wild-type (WT) and KO models. In a WT model (no KO), 8 different reactions were directly associated with Cer production. These reactions were maximized one-by-one (as the objective function), and fluxes were recorded. Consequently, these fluxes were converted to (%), which depicts the relative contribution of a reaction in the sphingolipid pathway toward Cer production. (%) of flux contributed by a reaction was relative to the total 'maximized' fluxes of all the neighboring reactions for Cer production multiplied by 100.

Next, we developed several KO models by iteratively removing a particular reaction (one at a time) of sphingolipid pathways, and simultaneously estimating the 'maximized' fluxes of neighboring reactions contributing directly toward Cer production. Likewise, the (%) of flux contributed by these reactions toward Cer production was estimated in a KO model. The KO analysis was performed using *'removeReactions'* function coded in the COBRA toolbox (v3.0)(Heirendt et al., 2017). All simulations were performed in MATLAB 2017b (Mathworks, Inc., Natick, MA, USA).